International Journal of Solids and Structures 322 (2025) 113632

Contents lists available at ScienceDirect

International Journal of Solids and Structures

journal homepage: www.elsevier.com/locate/ijsolstr

Yield surface and texture evolution in Ti-Cu Bimetal: Effects of tension and Tension-Cyclic torsion Pre-Deformation

Ved Prakash Dubey [a], Mateusz Kopec [a,c,*], Magdalena Łazińska [b], Zbigniew L. Kowalewski [a]

[a] Institute of Fundamental Technological Research, Polish Academy of Sciences, 5b Pawińskiego Str., Warsaw 02-106, Poland
[b] Faculty of Advanced Technologies and Chemistry, Military University of Technology, 00-908 Warsaw, Poland
[c] College of Science and Engineering, University of Derby, Markeaton Street, Derby DE22 3AW, UK

ARTICLE INFO

Keywords:
Yield surface
Plastic deformation
Bimetal
Texture evolution
Thin-walled tubular specimen

ABSTRACT

Investigating of the material properties and physical mechanisms responsible for plastic deformation caused by complex loading is crucial for bimetallic structures. These materials are a type of functionally graded multi-material structures designed to combine diverse material properties within the same framework while optimizing manufacturing costs. In the present work, the initial yield surface and its subsequent evolution were determined for a Ti-Cu bimetal based on the definition of yield stress for 0.01% plastic offset strain. The subsequent yield surfaces were determined after introducing monotonic axial tension and axial tension-cyclic torsion pre-deformation up to 1% permanent axial strain. It was found, that the determined initial yield surface was close to the Huber-von Mises-Hencky isotropic yield locus. Furthermore, subsequent yield surfaces were determined to assess a hardening/softening effect in the loading direction applied. Interestingly, only the monotonic tension caused a significant enhancement of the tensile yield strength as the monotonic tension associated with cyclic torsion caused its reduction. On the other hand, the sizes of subsequent yield surfaces reflecting pre-deformation were reduced in the axial compression direction. Finally, microstructural studies revealed, that only shear strain magnitude affects the yielding behaviour of bimetallic structure since more slip systems were activated when the higher strain magnitude was applied. Consequently, material recrystallization and subsequent softening in the radial direction (RD) occurred. The texture evolution is primarily interface-driven and deformation-mode dependent.

1. Introduction

The main objective in the design of structural metals is to manufacture high-strength materials characterized by improved the yield and ultimate strengths. Both these mechanical parameters immensely rely on the primary mechanisms of plastic deformation and evolving microstructure under loading conditions taken into account. In recent years, bimetals or two-phased nano-layered metals have been extensively investigated due to tremendous opportunities to replace costly and rare metals used in the industrial applications (Chen et al., 2022). Bimetals demonstrated higher strength and mechanical stability as compared to their component metals at extreme temperature and pressure environments (Gao et al., 2014). This unique behaviour of bimetals cannot be explained by a simple volumetric average property of the component metals.

A demand for bimetal joints made of two dissimilar metals has increased in many industrial applications due to the advantages of bimetal's attributes. As a result, it was anticipated, that such set of joints would be very useful in a variety of applications, including those involving the transportation sectors (automobile, rail, and aviation) as well as smaller, more frequently used items like saucepans for example (Sahasrabudhe et al., 2015; Tan et al., 2018). Such joint configurations can be fabricated using a conventional processing techniques, like a diffusion bonding (Ghosh and Chatterjee, 2005), friction welding (Beygi et al., 2018), explosive welding (Findik, 2011), and soldering (Yilmaz and Çelik, 2003). The mechanical properties of bimetals are significantly affected by the choice of fabrication technology and component materials. Therefore, it is necessary to investigate the behaviour of the bimetal formed during the combining process of metal layers, not only in uni-axial stress state, but also, under complex stress states in order to

* Corresponding author.
E-mail address: mkopec@ippt.pan.pl (M. Kopec).

https://doi.org/10.1016/j.ijsolstr.2025.113632
Received 2 June 2025; Received in revised form 21 July 2025; Accepted 23 August 2025
Available online 25 August 2025

simulate the conditions of real-world applications.

There have been numerous studies examining the mechanical properties of bimetal layered materials. Copper alloy – Austenitic stainless steel (SS316L) bimetallic structure fabricated using laser powder bed fusion (L-PBF) processing exhibited an average mechanical properties between those of the Cu alloy and SS316L. A higher strength of the bimetal in comparison to the copper alloy was associated to the formation of strong interface bonded due to interconnected network of steel and copper across the interface. Similar results also have been reported for copper-maraging steel bimetal, fabricated by L-PBF technique (Tan et al., 2018). A bimetallic structure consisting of Inconel 718 and copper alloy (GRCop-84), fabricated using the Laser Engineered Net Shaping (LENS^{TM}) technique, exhibited shear and compressive yield strengths of 220 MPa and 232 MPa, respectively. These values represent significant increases of approximately 100 % and 43 %, respectively, when compared to the corresponding strengths of the GRCop-84 base material. In contrast, the shear and compressive yield strengths of monolithic Inconel 718 were equal to 653 MPa and 712 MPa, respectively. The enhanced strength of the bimetallic structure relative to GRCop-84 is primarily attributed to the improved interfacial bonding, which results from the formation of a nickel-copper single-phase solid solution within the metallurgical bonding region (Onuike and Bandyopadhyay, 2019). In the case of bimetallic material consisting of aluminium alloy (Al6061) and mild steel, which was metallurgically bonded together using rotatory friction welding, the structure exhibited maximum tensile strength of 136 MPa, which was 65 % of the Al6061 base material (209 MPa) (Gotawala and Shrivastava, 2021). Similarly, the friction-welded bimetal consisting of aluminium alloy (AA6063-T6) and stainless steel (SS 304L) had reduced yield and tensile strengths of 156 MPa and 195 MPa, respectively. The values correspond to approximately 63 % and 72 %, respectively, of the strengths of AA6063-T6 base material (Vyas et al., 2021). The friction-welded titanium alloy (Ti-6Al-4 V) – LCS bimetal exhibited the tensile strength equivalent to 100 % of the LCS base metal's strength under specific conditions of high friction pressure, forge pressure and friction time (Kimura et al., 2016). The aforementioned material properties depend on the processing parameters. These parameters play a critical role in facilitating interatomic diffusion between the distinct materials, as a joining mechanism for achieving effective bonding. The formation of intermetallic compounds at the interface, which promotes localized brittle fracture, is a dominant factor for the observed lower joint strengths. Such compounds are well known for their potential to induce degradation of mechanical properties (Kimura et al., 2016; Lee et al., 2009).

It should be emphasized, that effect of plastic pre-deformation introduced through the uniaxial or complex loadings modes upon bimetallic structures remains a considerably unexplored domain. Till now, the primary focus of bimetal research has predominantly revolved around the optimization of its synthesis, either to take benefit on the distinctive properties of the constituent base materials or to selectively improve the overall properties of one of the base components. A recent investigation was carried out on the bimetallic aluminium – copper and steel – aluminium structures to describe the effect of plastic pre-straining, performed by the application of Equal Channel Angular Pressing-Drawing (ECAP-drawing). The results showed, that following four successive straining cycles (a cumulative 13.33 % reduction in diameter) of ECAP-drawing for the Al-Cu bimetal led to the enhancement of yield strength from 198 MPa to 515 MPa. Correspondingly, the tensile strength increased from 302 MPa to 689 MPa (Volokitina et al., 2023b). In the case of steel-aluminium bimetal, these properties increased from 260 MPa to 465 MPa and 370 MPa to 690 MPa, respectively, after two iterative strain cycles (a cumulative 10 % reduction in diameter) (Volokitina et al., 2023a). Such significant increments in the material strengths were mainly attributed to the grain refinement of materials after each pass and segregation of dislocations at the grain boundaries (Volokitina et al., 2023b).

In this work, a variation of mechanical properties of the as-received and plastic pre-deformed Ti-Cu bi-material was assessed. The yield surface approach was applied, since an evolution of the initial yield surface well illustrates the characteristics of plastic deformation. Numerous investigations have experimentally examined an evolution of subsequent yield surfaces for different single materials, such as Aluminium alloys (Du et al., 2023; Hong et al., 2022; Iftikhar et al., 2021; Ivey, 1961; Khan et al., 2010, 2009; Kowalewski and Turski, 2003; Lu et al., 2020; Naghdi et al., 1958; Phillips and Juh-Ling, 1972; Shiratori et al., 1976; Stout et al., 1985; Sung et al., 2011), Magnesium alloys (Iftikhar et al., 2022; Kabirian and Khan, 2015; Naka et al., 2008; Shi et al., 2017; Yang et al., 2019), Titanium (Dubey et al., 2023), Copper (Dietrich and Kowalewski, 1997; Hecker, 1971; Khan and Wang, 1993; Liu et al., 2023, 2018; Mair and Pugh, 1964), Brass (Helling et al., 1986; Miastkowski and Szczepiński, 1965; Phillips and Das, 1985; Shiratori et al., 1973), Steels (Dietrich and Socha, 2012; Hou et al., 2021; Hu et al., 2012; Ishikawa, 1997; Kim, 1992; Kowalewski et al., 2014; Kowalewski and Śliwowski, 1997; Kowalewski and Turski, 2003; Štefan et al., 2021; Wu and Yeh, 1991) and Inconel 718 (Gil et al., 1999). However, authors are aware of only one paper, by (Uscinowicz, 2013), that experimentally determined the yield surface of bimetallic structure (Al-Cu) and its evolution after uni-axial tensile plastic pre-strain. In the present paper, the yield surfaces of Ti-Cu bimetal in the as-received and after either monotonic uni-axial tension or simultaneous application of monotonic uni-axial tension – torsion – reverse torsion plastic pre-deformation, are presented.

There are four important reasons of the selected bimetal investigations in this work: (i) a functionally graded bimetallic system (Ti-Cu), which involves distinct material interfaces and plastic interactions between an HCP (Ti) and FCC (Cu) metal. This system exhibits unique mechanical responses and microstructural evolution mechanisms not observed in monolithic materials. The presence of an interface introduces complex stress transfer and recrystallization phenomena that are not present in homogeneous materials; (ii) prior studies on bimetallic structures are mainly focused on the improvement of its synthesis process and uniaxial mechanical properties. However, there is still a gap of comprehensive investigation of these bimetals under complex stress state, (iii) to the authors' knowledge, there are no such papers available up to now related to the yield surface identification of Ti-Cu bimetal and its evolution due to plastic pre-deformation under complex loading such as combined tension-cyclic torsion loading, and (iv) furthermore, apart from mechanical experiments, the authors decided to perform the EBSD measurements to reveal the deformation mechanisms responsible for yield surface evolution. The combination of the mechanical tests and microstructural investigations on bimetallic structures is thus important as the material behaviour under complex loading could be somehow explained by the detailed observations. Such studies were not reported as yet. These experimental results will be instrumental in formulating and validating analytical solutions for problems involving combined loading and yield criteria.

The paper is organized into four sections. Following this introductory part, Section 2 describes the Ti-Cu bimetal used in the study, including micrographs of the contact zone between layers. This section also presents the experimental techniques used for precise measurements, as well as those employed to investigate pre-deformation and yield surfaces. Section 3 discusses the experimental results, where the authors systematically examined the mechanical properties of the Ti-Cu bimetal through uniaxial tension and combined monotonic tension-cyclic torsion tests. The yield surfaces of the Ti-Cu bimetal, both in its as-received state and after pre-deformation from monotonic tension and various combinations of monotonic tension and cyclic torsion, are reported. These yield surfaces were determined using thin-walled tubular specimens subjected to sequential proportional loading paths, with the yield point defined by a designated plastic offset strain. Additionally, the texture evolution of the samples due to plastic pre-deformation was analysed. Finally, the conclusions are drawn in Section 4.

2. Materials and Methods

As-received material in the form of bimetallic solid rod consisting of two dissimilar component materials of a 9.4 mm diameter commercially pure copper (CP-Cu) core and a 1.6 mm thick shell of commercially pure titanium (CP-Ti) was investigated in this research. Initial bimetallic (Ti-Cu) rod with a nominal diameter of 12.6 mm and a length of 6 m was obtained by hot-extrusion of copper rod in titanium shell. The Ti-Cu bimetallic rod was hydrostatically extruded at the temperature of 700 °C, which allows for obtaining sufficiently high bonding strength without intermetallic compound at the interface. The bimetallic rod was not subjected to any heat treatment process after the extrusion. As reported in the literature (Lee et al., 2007; Matsushita et al., 1988), when the extrusion temperature was between 800 °C and 900 °C the formation of intermetallic compounds were observed at the interface of Ti-Cu which resulted in the reduction of bonding strength. Additionally, structural degradation at the interface of Ti-Cu has been reported due to the formation of intermetallic compounds after short-term annealing at temperature range from 600 °C to 900 °C (Uścinowicz, 2022). A scanning electron microscope (SEM) micrographs of the contact zone of Ti and Cu layers were shown in Fig. 1. There was no variation in microstructure and bonding quality along the hoop direction of the bimetal rod as could be observed in Fig. 1. The representative SEM images were presented for three locations marked I, II and III. It was observed, that there was a permanent connection of Ti and Cu metals without a transition layer and with no debonding nor significant differences in the joint area. Furthermore, chemical composition analysis was performed along the yellow line in area II to confirm the narrow joint area. As can be observed, there is no notable diffusion between titanium and copper since the reversible content of each element of almost 100 % could be found. The similar observations were performed in several places of the bimetal rod and since there was no significant difference, only representative results were shown.

Thin-walled tubular specimens were subjected to monotonic tensile loading as well as combination of monotonic tension – cyclic torsion. The main specimen dimensions were as following: gauge length of 16 mm, inner diameter of 8.4 mm, an outer diameter of 10.4 mm and an average thickness of 0.5 mm with variation of ± 17 μm of each material in the gauge section, as shown in Fig. 2a. The specimens were machined from the bimetallic rod of 12.6 mm diameter. Tensile characteristics were determined under constant strain rate of 0.005 s^{-1}. Tensile tests for the bimetal and its constituents were repeated three times to guarantee the reliability of the results obtained. Further, complex loading tests were performed on the thin-walled tubular specimens. The wall thickness of the tubular specimen was sufficiently large to satisfy the thin-walled tube criterion and to avoid buckling during complex loading. All the specimens were machined in a Computer Numerical Control (CNC) lathe machine to ensure precise dimensions of ± 0.01 mm. The microstructural analysis was performed by using Quanta 3D FEG field emission scanning electron microscope (SEM) operated at 20 kV. The samples for EBSD analysis were collected from the central part of the gauge area of thin-walled tubular specimens and were prepared by using the conventional metallographic procedures, including, grinding, initial polishing and electro-polishing. Fig. 2b presents a schematic of the specimen planes [Extrusion direction (ED) – Transverse direction (TD) – Radial direction (RD)] of the thin-walled tubular specimen for EBSD observations. In this work, EBSD scan was acquired for ED – RD plane.

All mechanical testing was performed on the MTS 858 servo-electrohydraulic biaxial testing machine with maximum capacity of ± 25 kN axial force and ± 100 Nm torque at room temperature (23 °C) controlled by the laboratory air-conditioning. Vishay 120 Ω strain gauges were bonded in the middle of the outer surface of gauge section of the thin-walled tubular specimens to measure and control axial, shear and hoop strain components. Due to torsional loading on the tubular specimens, the shear strain has a gradient across the thickness in the elastic range. It varies linearly from minimum value at the internal surface of the tube to the maximum one on its external surface. Despite the shear strain distribution is usually assumed to be uniform across the thickness if it is small, it should be noted that the external surface of the thin-walled tubular specimen represents a location of the most critical part. In order to mitigate the impact of strain gradient, the thickness of each metal in the gauge area was minimized to the maximum extent possible for conducting the experiment. During pre-deformation and yield probing, three-element 45° rectangular rosette EA-05-125RA-120 was used to measure the axial and shear strain, whereas linear pattern rosette EA-13-062AK-120 for the hoop strain. The gauges were bonded

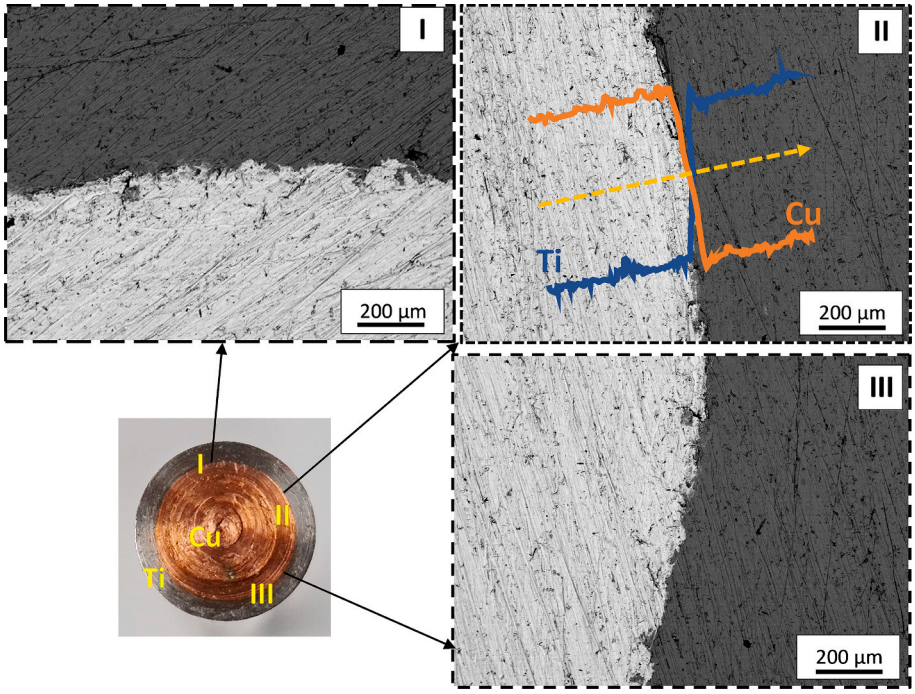

Fig. 1. SEM micrographs for the bonding quality examination in the hoop direction of Ti-Cu bimetal at various points in the as-received state.

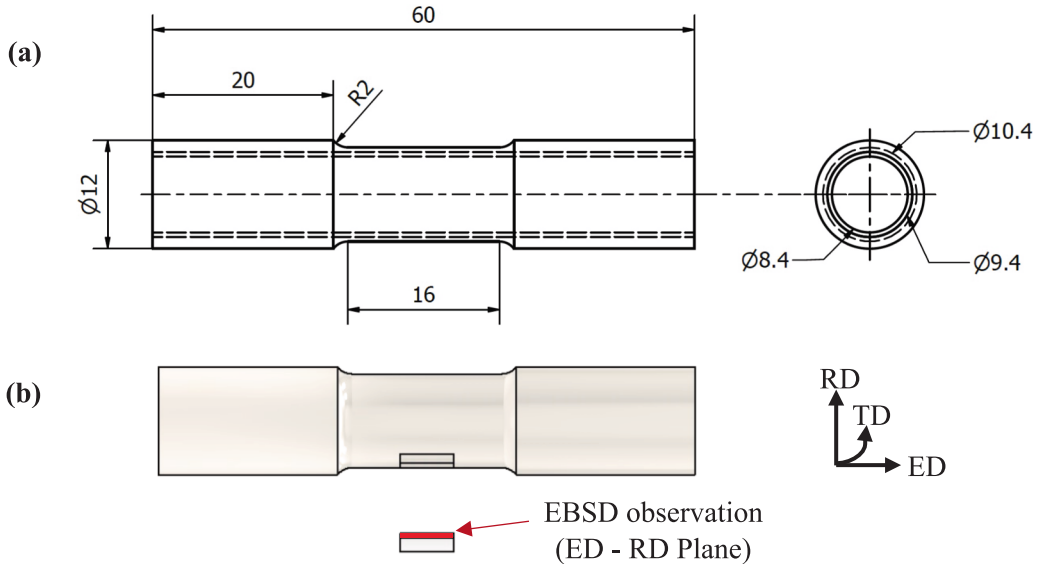

Fig. 2. Engineering drawing of the thin-walled tubular specimen (All dimensions are in millimetres) (a); scheme of the thin-walled tubular specimen planes for EBSD (b).

using M−Bond 610 adhesive produced by Measurements Group Inc. To assure the precise strain measurement and control of tests, strain gauges were arranged using methodology described in the authors previous work (Dubey et al., 2023).

The experimental studies involved four stages:

(1) determination of the basic mechanical properties of Ti-Cu bimetal;
(2) introduction of the following plastic pre-deformation in the specimens:
(a) monotonic tension up to 1 % permanent strain at constant strain rate of 5 x 10^{-6} s^{-1}.
(b) combination of monotonic axial tension up to 1 % permanent strain at constant strain rate of 5 x 10^{-6} s^{-1}, and proportional torsion-reverse-torsion cyclic loading for two magnitudes of strain amplitude (±0.1 % and ± 0.15 %) at two different values of frequency (0.5 Hz and 1 Hz).
(3) determination of the initial yield surface of the as-received material and yield surfaces of the pre-deformed material;
(4) determination of the microstructure and texture evolution after pre-deformation.

The selection of pre-strain parameters was influenced by material characteristics and experimental constraints with the objective of ensuring controlled deformation of the specimens. The strain gauges attached on the outer surface of the specimen, enabled a more precise control of the pre-deformation strain level compared to what can be achieved using the crosshead movement of the testing machine. The selection of a 1 % axial pre-strain level was based on the tensile stress–strain characteristics of the Ti-Cu bimetal and the strain gauge's operational range to ensure a limited axial plastic pre-strain value. Thorough investigation of combined monotonic tension with cyclic torsion for different values of the shear strain amplitude, revealed that bimetal failed to get the desired axial strain level, reaching up to shear strain amplitude of ± 0.4 % at frequency of 0.5 Hz. It shows that the interface of bimetal is very sensitive to the values of cyclic shear strain amplitude. Therefore, to introduce a stable pre-deformation level during the bi-directional loading conditions, the magnitude of cyclic shear strain amplitude was taken to be equal to ± 0.1 % and ± 0.15 % and frequency of 0.5 Hz and 1 Hz. Under these loading conditions axial deformation up to 1 % could be successfully executed.

The detailed experimental setup and probing methodology have been comprehensively outlined in previous work of (Dubey et al., 2023). However, for the completeness, a concise overview of the probing methodology to determine the yield loci in this study is given below. The concept of yield surfaces within the axial-shear stress space (two-dimensional space) was implemented to assess the effect of plastic pre-deformation on the bimetal by examining the yield points. It is important to note, that after prior tension or combined tension–torsion plastic pre-deformation, all specimens were subjected to a relaxation period at the zero-stress state for 1 h. Subsequently, they were subjected to the yield surface determination procedure. The relaxation step was incorporated to mitigate the influence of different strain rates during pre-deformation and probing of yield surface. For each state of the material (as-received and pre-deformed), yield points for each yield surfaces were determined using a single specimen approach. The use of a single specimen to determine yield points provides a major advantage by eliminating inter-specimen variability in geometry, microstructure, and boundary conditions. This methodology resulted in a total set of six specimens. A sequential probing technique was employed for the determination of yield points, involving 16 distinct strain paths. The sequence started with simple tension and finished with tension along the same direction within the (ε_{xx}, $\sqrt{(3/(1+\nu)^2)}\varepsilon_{xy}$) strain plane (refer to Fig. 3), where ν denotes Poisson's ratio. For each path, strain-controlled loading was initiated from the origin, progressing until a limited plastic offset strain of 1 x 10^{-4} (0.01 %) was reached. Subsequently, the stress-controlled unloading was conducted until zero force and torque were achieved. The 0.01 % plastic offset was selected to ensure a clear and reproducible identification of the onset of plasticity under multiaxial loading conditions while considering the instrument resolution, noise sensitivity and yield point ambiguity, especially in axial-shear stress space where path curvature may affect onset interpretation.

Probing order was symmetrically distributed across the biaxial stress space to avoid biasness. Using 16 probing paths in axial-shear stress space offers significantly higher angular resolution, enabling accurate reconstruction of the yield surface's shape, especially in regions exhibiting curvature, distortion, or anisotropy. This dense sampling improves detection of yield surface translation and directional hardening effects that may be missed with fewer directions. Additionally, the increased

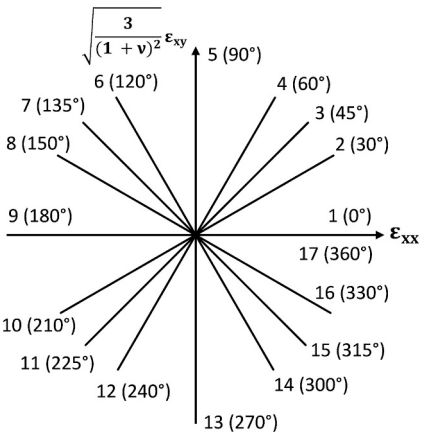

Fig. 3. Loading sequence of strain paths for yield points determination in the biaxial strain space.

number of points supports more accurate parameter identification and avoid overfitting or misrepresentation due to under-sampled data for an advanced constitutive models, such as those incorporating distortional or kinematic hardening.

Throughout all tests, the stress state components for thin-walled tubes were defined by the following general formula to specifically estimate the stresses at the outer surface assuming average stress over the wall, but also recognizing that this point corresponds to where the strain gauges were applied in our experimental setup:

$$\sigma_{xx} = \frac{4F}{\pi(D^2 - d^2)} \tag{1}$$

$$\tau_{xy} = \frac{16TD}{\pi(D^4 - d^4)} \tag{2}$$

The magnitude of the equivalent stress in the stress state considered was expressed by the well- known relationship:

$$\sigma_{eq} = \sqrt{\sigma_{xx}^2 + 3\tau_{xy}^2} \tag{3}$$

The equivalent strain was determined from a generalized form of the von Mises equivalent strain based on the strain energy equivalence principle and incorporates Poisson's ratio ν to account for material compressibility. This formulation ensures that the internal energy computed from the scalar equivalent quantities matches the energy obtained from the full tensorial stress–strain components.

$$\varepsilon_{eq} = \frac{\sqrt{2}}{2(1+\nu)}\sqrt{(\varepsilon_{xx} - \varepsilon_{yy})^2 + (\varepsilon_{yy} - \varepsilon_{zz})^2 + (\varepsilon_{zz} - \varepsilon_{xx})^2 + 6\left(\varepsilon_{xy}^2 + \varepsilon_{yz}^2 + \varepsilon_{zx}^2\right)} \tag{4}$$

when the value of ν equal to 0.5, the material behaves as perfectly incompressible, and Equation (4) reduces to the classical von Mises equivalent strain expression. A full derivation is provided in Appendix A.

The experiments were performed in the plane stress conditions, which leads with:

$\varepsilon_{yy} = \varepsilon_{zz} = -\nu\varepsilon_{xx}$ and $\varepsilon_{yz} = \varepsilon_{zx} = 0$ to the relationship

$$\varepsilon_{eq} = \sqrt{\varepsilon_{xx}^2 + \frac{3}{(1+\nu)^2}\varepsilon_{xy}^2} \tag{5}$$

The equivalent plastic strain was determined using the following relation based on the additive decomposition of total strain in the framework of classical small-strain plasticity:

$$\varepsilon_{eq}^p = Equivalentstrain - Equivalentelasticstrain \tag{6}$$

This approach assumes isotropic plasticity and associated flow under proportional loading, where the stress and strain tensors evolve along a common path, and the plastic flow direction remains aligned with the deviatoric stress. It should be pointed out that, while this scalar-based formulation is widely used in engineering applications, it does not fully reflect the tensorial nature of strain decomposition, especially under non-proportional or complex multiaxial loading paths. In such cases, a more rigorous computation involving incremental plastic strain accumulation based on the plastic strain rate tensor would be required. Nonetheless, for the material system and proportional loading paths (Fig. 3) considered in this study, the formulation provides a practical and reasonable estimation of equivalent plastic strain.

The Poisson's ratio was determined using the following relation:

$$\nu = -\frac{Circumferentialstrain}{Axialstrain} \tag{7}$$

To accurately capture the initial stiffness response under a combined axial and torsional loading conditions, the effective Young's modulus was determined based on the slope of the initial linear region of the equivalent stress-equivalent strain curves corresponding to each loading path employed in the yield point determination, as illustrated in Fig. 3. It quantifies the stiffness of a material and is defined as:

$E_{eff} = \frac{\sigma_{eq}}{\varepsilon_{eq}}|$initial linear region (8)where, σ_{xx} – axial stress; F – axial force; D – initial outer gauge diameter of the specimen; d – initial inner gauge diameter of the specimen; τ_{xy} – shear stress; T – twisting moment; σ_{eq} – equivalent stress; ε_{eq} – equivalent strain; ε_{xx} – axial strain; ε_{xy} – shear strain; ε_{eq}^p – equivalent plastic strain; E_{eff} – effective Young's modulus; ν – Poisson's ratio and ε_{yy} – circumferential (hoop) strain.

The classical Young's modulus is defined as the initial linear elastic slope of the stress–strain curve under uniaxial loading, and that the term "equivalent or effective Young's modulus" is commonly used in the context of composite or heterogeneous materials to represent a homogenized stiffness response derived from the properties of individual constituents. However, in the present work, the effective Young's modulus is not intended to represent the intrinsic elastic modulus of a single material phase (Ti or Cu), nor a weighted average based on rule-of-mixtures. Instead, it reflects the apparent elastic stiffness of the entire bimetallic structure (Ti-Cu layered system) when subjected to a multiaxial loading path. This value is measured only within the elastic regime of the equivalent stress–equivalent strain response, avoiding the influence of plasticity, softening, or strain hardening behaviour, thereby maintaining its correspondence with the elastic modulus concept, though in an equivalent multiaxial loading condition. This approach is necessary due to the non-uniaxial, multiaxial stress state, the directional interactions between layers, and the complex geometry and boundary conditions inherent in the test configuration.

For the bimetal tested, the experimentally determined average value of the Poisson's ratio was equal to 0.3. It has to be emphasized that above expressions were only used to control all the tests, i.e. to obtain a defined pre-strain value. Therefore, they did not influence the real response of the material to the loading program applied.

Yield points were determined using the designated offset strain method, with yield being defined as the point at which the equivalent stress–strain curve deviated by 0.01 % from the elastic line for each loading direction. When a single specimen is used to determine the yield surface, it is recommended to employ a small plastic offset strain for the yield definition. The reason for this is that the accumulation of additional plastic strain from the prior loading path should be minimal in order to be considered negligible. Szczepinski anisotropic yield condition was applied for the numerical calculation of yield surface (Szczepinski, 1993). To fit the experimental yield points by the Szczepinski anisotropic yield equation, the least squares method was used. The aforementioned methodology was applied to determine the initial and subsequent yield surfaces.

3. Results and discussion

3.1. Basic mechanical parameters of the material

The basic mechanical properties governing the elastic and plastic properties of the Ti-Cu bimetal were determined using data captured from uniaxial monotonic tensile tests. The values obtained from these tests were extremely important in the experimental planning for pre-deformation processes and probing of yield surfaces. Tensile tests were performed on the Ti-Cu bimetal specimen, and its constituents' metals, namely titanium (Ti) and copper (Cu), independently. The tensile properties of the Ti-Cu bimetal, along with CP-Ti and CP-Cu, were determined on the basis of their respective stress–strain curves (Fig. 4a) and they were listed in Table 1. The constituent metals undergo different heat treatment processes in comparison to the Ti-Cu bimetallic material. Data in Table 1 presents the tensile mechanical properties of Ti-Cu bimetal, enables a direct comparison with that of CP-Ti and CP-Cu. The copper bars used in this study were obtained in the M1E-Z4 condition, which corresponds to the Cu-ETP (M1E; E-Cu58) state. This state is achieved by annealing the copper bars at temperatures ranging from 350 °C to 600 °C. On the other hand, the titanium bars are classified as grade 2 (3.7035/UNS R50400/ASTM B348 EN10204/3.1) and undergo a sequence of heat treatments. This includes a process of soft annealing at temperatures between 600 °C and 700 °C, followed by stress relief heat treatment within the range from 450 °C to 600 °C. Based on the tensile test results, some insightful parallels could be drawn for strength characteristics between the constituent materials and the bimetal. It became evident, that the bimetal's tensile yield and ultimate strengths fell within the spectrum defined by copper and titanium, each serving as reference materials to set the baseline for strength characteristics within the bimetal. The yield strength of bimetal was about 43 % higher and 6 % lower than Cu and Ti, respectively. However, the ultimate strength was about 50 % higher and 23 % lower of them. This notable improvement in the strength of the bimetal was necessary in ensuring the mechanical reliability of the joint and was attributed to the accumulation of particles and elemental diffusion near the interface (Onuike and Bandyopadhyay, 2019). One can indicate however, that the ductility of bimetal was lower than its constituent metals. Similar results have been also reported for Al-Cu bimetallic joint processed using rolling after heating the metals (Uscinowicz, 2013).

Fig. 5 shows the fractography of the Ti-Cu bimetal, CP-Ti and CP-Cu specimens, fractured during uniaxial tensile testing. Since titanium exhibited almost doubled elongation as copper (Fig. 4a), the fracture behaviour of bimetal was different. It could be observed, that the thickness of the titanium part of the specimen is relatively uniform, while that for the copper varies due to the elongated neck observed in the axial direction, as shown in Fig. 5a. One should mention, that both materials exhibit ductile behaviour (Fig. 5b and 5c) when the specimens of constituent metals are deformed separately. The fracture areas of both, titanium and copper, are characterized by dimples and micro-voids formed during plastic deformation. Because the bimetal consists of materials of different strength properties, the copper is starting to fracture much earlier than titanium. Such behaviour leads to the debonding of two metals since the hydrostatic extrusion process enables a bond which is able to withstand the shear of ~ 150 MPa (Uścinowicz, 2022).

Table 1
The mechanical properties of bimetal and its constituent metals.

Material	0.2 % Yield strength [MPa]	Tensile strength [MPa]	Elongation [%]	Young's modulus [GPa]
Bimetal (Ti-Cu)	377 (± 2)	410 (± 1)	18 (±0.5)	106 (±1)
Titanium	400 (± 3)	531 (± 1)	37 (±1.2)	100 (±1)
Copper	264 (± 2)	274 (± 1)	21 (±1.4)	110 (±1)

3.2. Equivalent mechanical parameters of the material tested under combined loading

The material characteristics were systematically compared to the Ti-Cu bimetal specimen, which was subjected to distinct loading conditions: uniaxial tension, tension–torsion, and pure torsion. The equivalent stress-equivalent strain curves in Fig. 4b represent these results. All three curves in Fig. 4b start at the origin, uniaxial tension and tension–torsion curves nearly coincide, whereas, pure torsion curve differs a little. Notably, the values of effective Young's modulus in various loading directions presented in Fig. 7, underline that the lowest Young's modulus is associated with pure torsion loading. This observation signifies the intrinsic variability in material characteristics under different loading conditions for the Ti-Cu bimetal. These differences are presumably attributed to the initial anisotropy introduced into the material during the manufacturing process.

3.3. Material behaviour under complex cyclic loading

The study examined how the Ti-Cu bimetal behaved under monotonic stress when subjected to cyclic torsion with a range of strain amplitudes and frequencies. Two primary objectives of these experimental investigations can be indicated: to induce plastic pre-deformation within the material, and to examine the changes in tensile characteristics resulting from the application of torsion-reverse-torsion cycles. Fig. 6a and 6b present the axial engineering stress–strain curves, highlighting how increasing the cyclic strain amplitude and frequency leads to a gradual reduction in axial tensile stress. This stress reduction reflects a material softening response as the cyclic shear deformation intensifies.

To better understand the influence of torsional shear on the overall material response, Fig. 6c–6f present the equivalent von Mises stress–-strain curves, calculated by integrating both axial and torsional stress components. It is evident from the trajectories of the equivalent stress–strain curves, that bimetal demonstrate a softening effect as the amplitude of cyclic torsional strain increases. The same effect has been reported for commercially pure Ti (Dubey et al., 2023) and commercially pure Cu (Zhou et al., 2022), and was attributed to the development

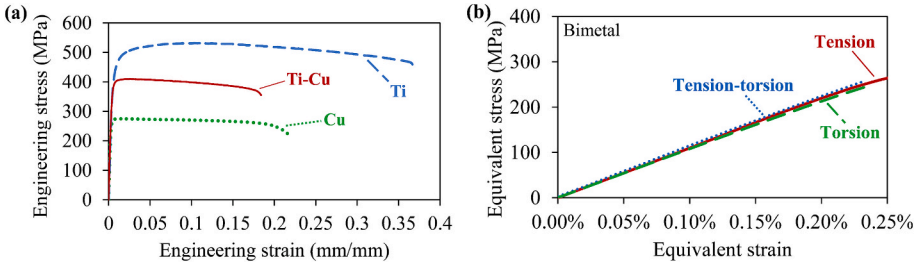

Fig. 4. Tensile stress–strain characteristics of thin-walled tubular specimens of Ti-Cu bimetal; and its constituent metals (pure titanium and copper) (a); Comparison of material characteristics of bimetal for different loading paths on thin-walled tubular specimen (b).

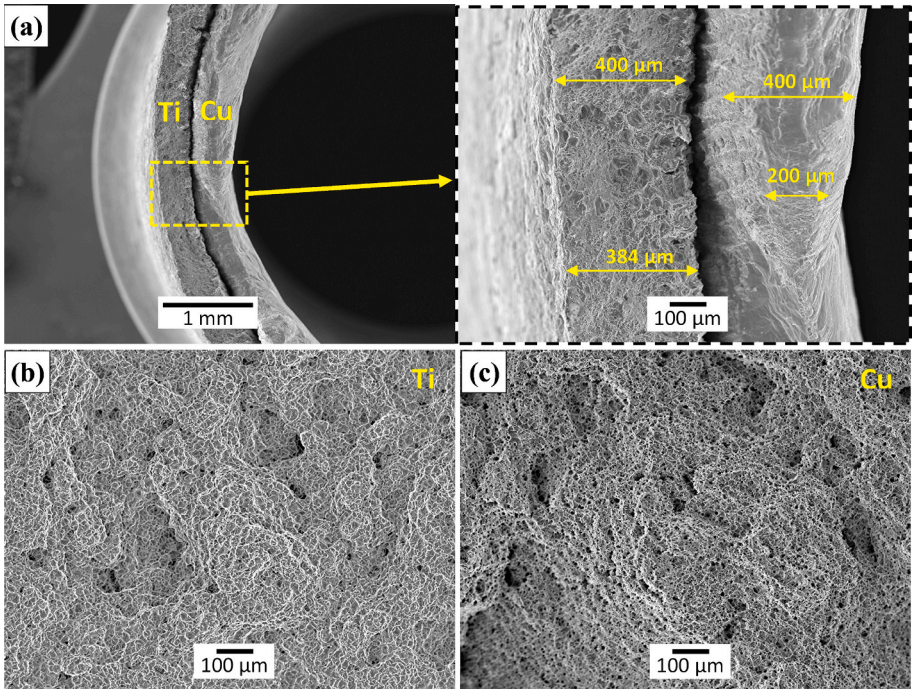

Fig. 5. SEM micrographs of the tensile deformed Ti-Cu bimetal with magnified view (a); the tensile deformed CP-Ti (b) and CP-Cu (c).

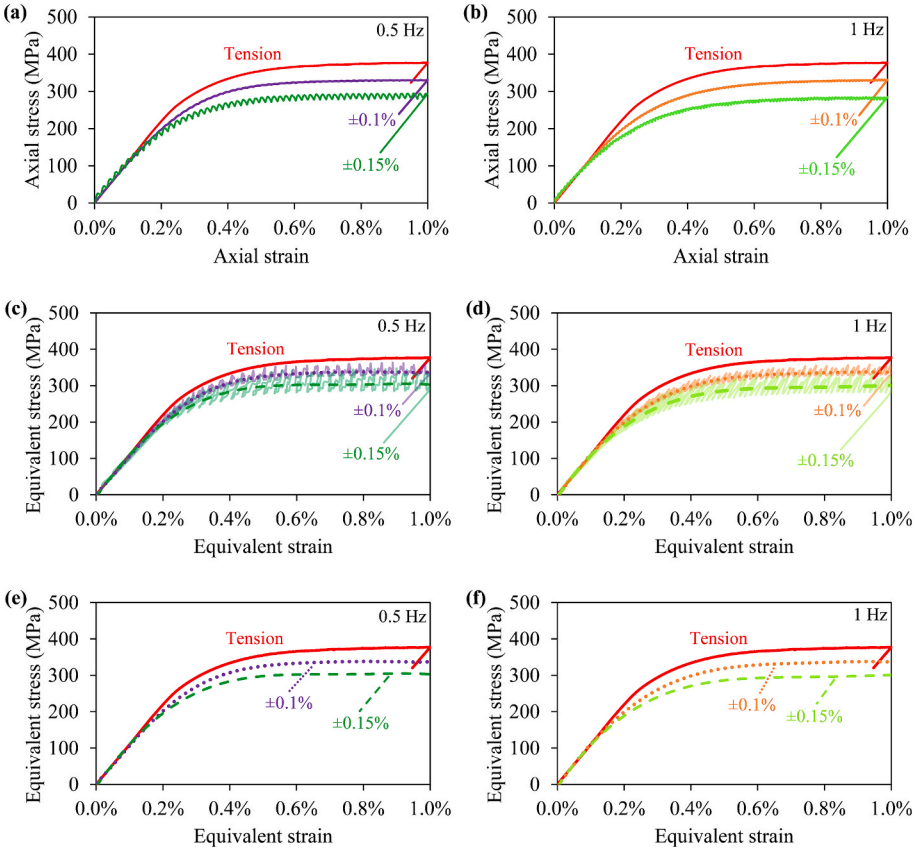

Fig. 6. Axial engineering stress–strain curves (a, b) and equivalent stress–strain curves (c, d, e, f) of Ti-Cu bimetal subjected to: monotonic tension only and simultaneous application of monotonic tension with cyclic torsion with strain amplitude equal to: ± 0.1 % and ± 0.15 % at frequency of 0.5 Hz and 1 Hz, respectively.

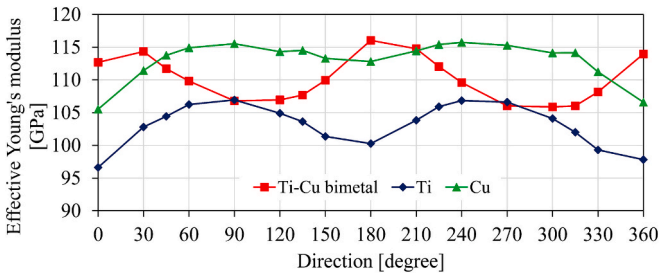

Fig. 7. The effective Young's modulus values of the Ti-Cu bimetal and its constituent metals in various loading directions in the strain plane considered.

of specific crystallographic textures in titanium and more elongated sallow dimples on the copper fracture surface during combined tension–torsion loading.

3.4. Determination of the yield surface for bimetal in the as-received state

Elastic properties of the tested bimetal and its constituent metals (pure titanium and copper) were presented in the form of effective Young's modulus values obtained for each specific direction (Fig. 7). These values were different depending on the loading direction in the strain plane considered. The value of Young's modulus of Ti-Cu bimetal exhibited a maximum in the direction of 180°, which corresponded to the pure compression. On the other hand, the lowest value of Young's modulus was observed during pure torsion (direction 270°). Although the discrepancy between the minimum and maximum values of this parameter was approximately 9 %, which from a practical point of view can be considered as small, it nevertheless highlights the presence of the material texture even in the as-received state. Determination of material texture relies on a comprehensive analysis of characteristics across all considered directions. The potential reason of the Young's modulus values dispersion was associated with strongly oriented texture.

Additionally, Fig. 7 shows that the effective Young's modulus of Ti-Cu bimetal is close to or slightly higher than that of pure Cu under pure axial loading (tension and compression). This suggests that the Cu layer primarily governs the mechanical response in axial-dominated directions. In contrast, under pure torsional and reverse torsional loading, the bimetal's Young's modulus closely matches that of pure Ti, indicating that the Ti component controls the response in shear-dominated directions. In intermediate loading directions, the stiffness of the bimetal transitions between those of its constituents, reflecting a direction-dependent mechanical behaviour. Pure Ti demonstrates notable anisotropy, with lower Young's modulus values in pure axial directions and higher values under torsional loading, highlighting its greater stiffness in shear. Pure Cu, meanwhile, shows relatively consistent Young's modulus values across all directions, with a mild anisotropic response and generally higher stiffness than Ti. The Ti-Cu bimetal effectively blends the mechanical characteristics of both metals, which underscores its potential advantage in applications involving complex or multidirectional stresses.

For the relatively low magnitude of plastic strain introduced in the study, such variations in the Young's modulus can exert a notable influence on the results of yield surface analysis, particularly when a single Young's modulus value from the monotonic tension would be applied for all loading directions taken into account. To mitigate this limitation, the authors adopted an approach, that employs the effective Young's modulus value specific to each respective stress direction. This methodology accounts for the inherent elastic anisotropy and its consequential impact on the accurate estimation of plastic strain during testing along various stress directions. Through this refined approach, the authors aim to enhance the precision and robustness of the analysis by comprehensively addressing an influence of elastic anisotropy on the plastic strain estimation.

The yield surfaces of the as-received Ti-Cu bimetal were shown in Fig. 8a as ellipses. They were determined by fitting the yield points using the least square method in the Szczepinski anisotropic yield equation (Szczepinski, 1993) obtained at 0.005 % and 0.01 % plastic offset strain in each loading directions of the plane strain state. The yield surfaces determined demonstrate an impact of the selected yield point definition. The yield stress at 0.01 % plastic offset strain was found to be 221.25 MPa in tension and −200.8 MPa in compression. It exposes the presence of tension–compression asymmetry in the Ti-Cu bimetal. The yield stresses in torsion and reverse torsion were equal to 141.08 MPa and −140.77 MPa, respectively, for same offset strain. Similar results have also been reported in the literature (Iftikhar et al., 2022; Kabirian and Khan, 2015). The parameters characterising the ellipses are presented in Table 2. They represent the initial yield surfaces of the Ti-Cu bimetal, corresponding to both selected offset strain values. The yield surfaces of the bimetal in the as-received state are shifted in the tension direction, and the axes ratios are considerably lower than 1.73, which is the value for the isotropic material according to the Huber – von Mises – Hencky yield criterion (Huber, 1904; von Mises, 1913; Hencky, 1924). Such behaviour indicates an occurrence of the initial anisotropy.

The theoretical isotropic yield surface was determined in order to perform precise comparison with the yield surface of Ti-Cu bimetal captured experimentally. It was achieved by aligning the yield point in tension (designated as direction 0) with that of the 0.01 % offset for the initial yield surface of bimetal. According to the Huber – von Mises – Hencky yield criterion, the resulting isotropic yield surface is centred at the origin, displayed a zero-degree rotation angle, and maintained the

Table 2
Ellipse parameters for the initial yield surface of Ti-Cu bimetal.

Definition of yielding	Centre ($\mathbf{x}_0$, $\mathbf{y}_0$) [MPa]	Rotation angle (∅) [Radian]	Semi-axes (**a**, **b**) [MPa]	Axes ratio (**a**/**b**)
0.01 % offset strain	8.25, −1.76	0.11	225.31, 145.64	1.55
0.005 % offset strain	4.78, 0.03	0.16	205.18, 146.10	1.40

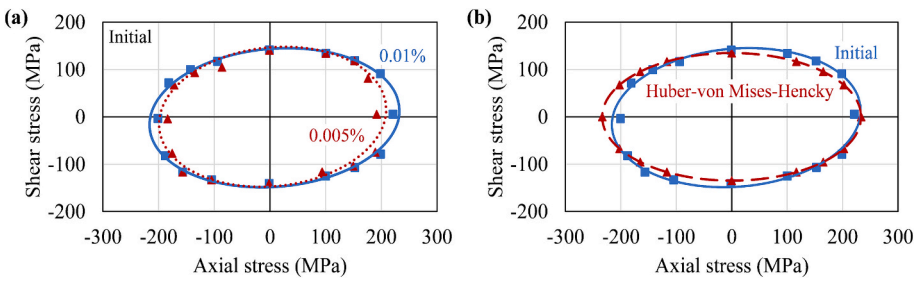

Fig. 8. Yield surfaces of Ti-Cu bimetal in the 'as-received' state with yield points (square and triangular points) obtained for 0.01% and 0.005% plastic offset strains (a); Initial yield surface (0.01% offset strain) of the Ti-Cu bimetal compared with the Huber-von Mises-Hencky isotropic yield locus (b).

axes ratio of 1.73. Fig. 8b shows how the isotropic yield surface was configured. It can be observed, that the broken line representing the predicted Huber – von Mises – Hencky yield locus is nearly similar to that obtained experimentally for the Ti-Cu bimetal, except of the compression direction. It reflects a characteristic softening that corresponds to the compressive strength reduction. Such behaviour can be attributed to the preferred texture or grain orientation in the as-received state of bimetal.

Fig. 9 shows a comparison of the initial yield surface of Ti-Cu bimetal with those of CP-Ti and CP-Cu. Each yield surface corresponds to the onset of plastic deformation for 0.01 % plastic offset strain. The yield surface of CP-Ti is the largest, indicating that it has the highest yield strength among the three materials in both axial and shear directions. In contrast, CP-Cu has the smallest yield surface, reflecting its lower yield strength in both loading modes. The Ti-Cu bimetal exhibits a yield surface that lies between those of its constituents, showing intermediate yield strength characteristics. This intermediate yielding highlights the synergistic effect of combining Ti and Cu, where the bimetal inherits the higher axial strength of Ti and moderate shear strength closer to Cu. Additionally, the results suggest that the Ti-Cu bimetal can be effectively engineered for improved performance under multiaxial loading conditions. This combined response offers a favourable balance of mechanical strength, economic efficiency, and application versatility that surpasses what either CP-Ti or CP-Cu can achieve individually.

3.5. Determination of the yield surface for the pre-deformed material

The subsequent yield loci were determined for 0.01 % plastic offset strain in tension–torsion stress space following monotonic tension and various combinations of the tension-cyclic torsion plastic pre-deformation, using the same procedure as applied to the material in the as-received state. An effect of plastic pre-deformation on the bimetal was evaluated based on the evolution of the initial yield surface. All specimens were subjected to pre-deformation until they reached an axial strain of 1 %.

The yield locus and yield points corresponding to bimetal subjected to 1 % tensile pre-deformation is presented in Fig. 10, as denoted by the dashed line and triangles. It can be clearly seen, that the shape of the yield surface exhibits significant shift towards the tensile direction, i.e. direction of prior deformation. It indicates, that the application of monotonic tensile deformation led to the induction of kinematic hardening within the bimetallic structure. Specifically, the yield point in tension increased from 221 MPa to 288 MPa and that in compression decreased from −201 MPa to – 150 MPa, representing close to 30 % and 25 % variation in comparison to the initial values, respectively.

Fig. 11 illustrates the fitted yield loci and experimentally obtained yield points of plastically pre-deformed Ti-Cu bimetal due to monotonic tension assisted by torsion-reverse-torsion of various strain amplitudes

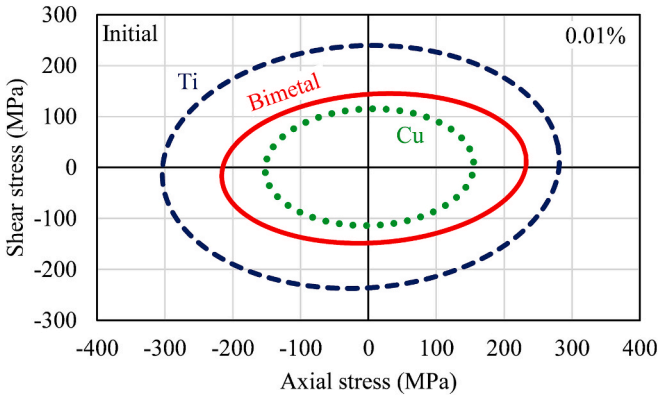

Fig. 9. Initial yield loci of Ti-Cu bimetal, CP-Ti, and CP-Cu obtained for 0.01% plastic offset strain.

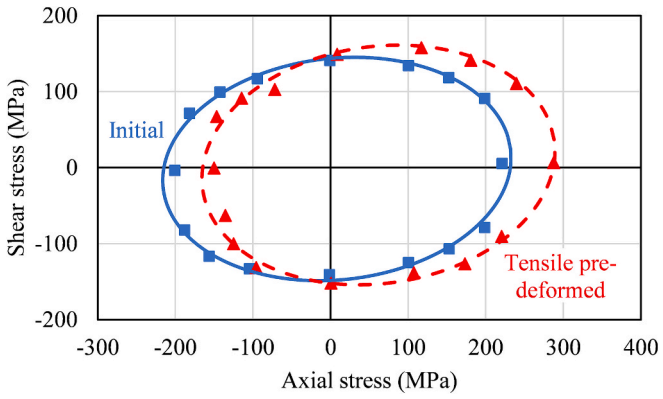

Fig. 10. Comparison of the yield surfaces for tensile pre-deformed Ti-Cu bimetal and the same material in the as-received state.

and frequencies. These subsequent yield surfaces were shown in comparison to the initial yield surface of the tested material (represented by a continuous line). The results identified clear anisotropic softening of the bimetal. Specifically, for the cyclic torsional strain amplitude equal ± 0.1 % at frequency of 0.5 Hz (Fig. 11a) and 1 Hz (Fig. 11c), the subsequent yield surfaces exhibited a decrease of 14 % in the tensile yield stress for both cases and a decrease of 17 % and 20 % in the compressive yield stress, respectively, as compared to those representing the initial yield point values. It has to be indicated however, that the yield stresses in torsion and reverse torsion exhibited an equal slight reduction of 6 % for both values of cyclic loading frequency applied in this work.

When the cyclic strain amplitude was increased from ± 0.1 % to ± 0.15 % for monotonic tension assisted by cyclic torsion pre-deformation, the size of the yield surfaces was reduced in all directions, however, more dominantly in the compressive direction, at frequency of 0.5 Hz (Fig. 11b) and 1 Hz as well (Fig. 11d). A decrease of the tensile yield stresses was 9 % and 7 % at 0.5 Hz and 1 Hz, respectively, whereas of the compressive yield stresses 27 % and 28 %, respectively. Additionally, yield stresses in torsion and reverse torsion showed an equal decrease of nearly 13 % for monotonic tension assisted by cyclic torsion of strain amplitude equal to ± 0.15 % at frequency of 0.5 Hz (Fig. 11b) and nearly 22 % decrease in both stresses at an increased frequency of 1 Hz (Fig. 11d). One should note that, regardless of the level of pre-deformation introduced through combined monotonic tension-cyclic torsion, a significant decrease of the compressive yield stress and noticeable reduction of the shear yield stress were observed in the Ti-Cu bimetal, particularly for higher cyclic torsion strain amplitude. The rate of anisotropic softening increased with the increase of combined pre-deformation level. This softening behaviour is primarily driven by shear-induced microstructural changes, particularly in copper (detailed investigation is reported in Section 3.6). Despite many previous investigations performed on the impact of pre-deformation on materials, relatively few studies explored this phenomenon from the perspective of yield surface evolution. A similar tendency of kinematic hardening variation after 1 % tensile pre-strain (Fig. 10) was observed in CP-Ti (Dubey et al., 2023) and various steels (Štefan et al., 2021). This behaviour was attributed to factors such as preferred texture and the presence of non-shearable, incoherent precipitates, which hinder the dislocation motion. The increased tensile yield strength (+30 %) and decreased compressive yield strength (−25 %) confirmed this effect, resembling the response of titanium (Dubey et al., 2023), which dominates the outer layer of the tubular specimen and hence governs the response under axial loading. It has to be emphasised, that the effects associated to influence of monotonic tension assisted by cyclic torsion on the yield surface has received relatively limited attention up to now. The softening effect identified by subsequent yield surfaces was also observed in other materials, including 18G2A low alloy steel

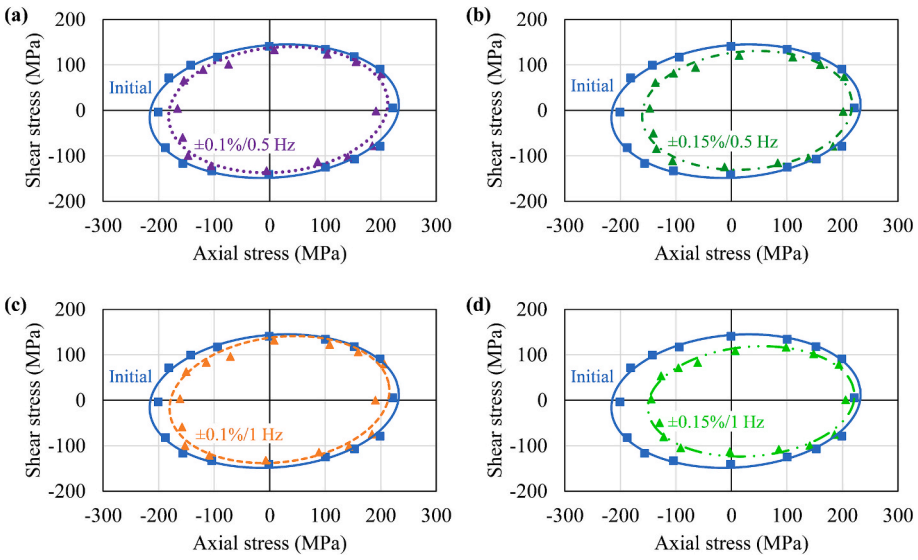

Fig. 11. Comparative analysis of the initial yield surface of the Ti-Cu bimetal with the yield surfaces of the same bimetal subjected to pre-deformation through the combined monotonic tension and cyclic torsion of strain amplitude equal to ± 0.1 % and ± 0.15 % at frequencies of 0.5 Hz (a, b) and 1 Hz (c, d), respectively.

(Kowalewski and Śliwowski, 1997) and A336 GR5 structural steel (Dietrich and Socha, 2012), following the application of cyclic pre-strain history.

The experimentally obtained yield points were fitted by the Szczepinski yield function (Szczepinski, 1993) using the least squares method to describe the ellipse representing the approximate yield surface of the tested material. In Table 3, the fitting errors, computed through the minimization of the sum of squares of the distances of the experimental yield points from the approximated yield surface, were presented for each of the yield surfaces determined. These fitting error values, in each case, were found to be exceptionally minimal. This observation indicates a precise match between the experimental data and the fitted elliptical approximation. The consistently low fitting errors confirm the suitability and high accuracy of the yield surface equation, as well as the overall quality of the yield surface approximation.

Fig. 12 provides the variation in the parameters characterising the elliptical shape of the yield surface (YS) for the Ti-Cu bimetal in the pre-deformed state. It should be noted, that pre-deformation due to monotonic tension is represented by 0 % strain amplitude as shown in Fig. 12. The results present, that the semi-axes (a, b) of the yield surface of material pre-deformed due to monotonic tension increased to 228.73 MPa and 155.65 MPa in comparison to that of the as-received state (225.31 MPa, 145.64 MPa). On the other hand, these values decreased after the combined pre-deformation at both frequencies considered (0.5 Hz and 1 Hz) (Fig. 12a and 12d).

The axes ratio of the subsequent yield surfaces was compared with two reference frameworks: the initial yield surface, as presented in Table 2, and the Huber – von Mises – Hencky isotropic yield surface. Such comparison was presented in Fig. 12b and 12e. It could be observed, that the axes ratio of the yield surface was nearly constant after all pre-deformation level considered, except of that determined after monotonic tension-cyclic torsion with strain amplitude of ± 0.15 % at 1 Hz, which closely resembles the axes ratio of as-received state. The rotation angle (Ø) of the yield surface axes with respect to the axial-shear stress co-ordinate system showed the variation with pre-deformation level. The maximum value of 0.19 rad rotation was observed after the monotonic tension assisted by cyclic torsion with strain amplitude of ± 0.1 % at frequency of 1 Hz (Fig. 12c and 12f).

Fig. 13 provides a comprehensive visualization of the initial yield surface evolution in the axial-shear stress space, following various level of pre-deformation of the Ti-Cu bimetal. It was observed, that each yield surface has a distinct shape and the size of subsequent yield surfaces decreases in the compressive direction, which is the opposite of that representing the tensile pre-deformation of bimetal. The yield surface of bimetal after 1 % monotonic tension pre-deformation exhibited the largest dimensions. By examining Fig. 13a and 13b, it becomes evident that:

- monotonic tension pre-deformation leads to the kinematic hardening in the same direction as that used during pre-deformation;
- combined monotonic tension-cyclic torsion pre-deformation leads to the kinematic softening in all directions and it becomes more prominent with the increase of torsional strain amplitude.

One could observe the impact of an increase of cyclic torsional strain amplitude on the yield surface in Fig. 13. The yield surface obtained after monotonic tension-cyclic torsion with a strain amplitude of ± 0.15 % pre-deformation exhibits a similar tensile yield stress compared to that obtained for ± 0.1 % torsional strain amplitude. On the other hand, a significant decrease in all other stress directions could be found. Similar tendencies can be observed for both frequencies (0.5 Hz and 1 Hz) used in the pre-deformation process. An examination of the shape of these subsequent yield surfaces elucidates, that the dimensions of the yield surface are dependent upon the nature of the pre-deformation process.

The reported yield surface evolution reflecting the effect of plastic pre-deformation of Ti-Cu bimetal is compared with those of copper and titanium present in the literature. The 99.9 % pure copper exhibited isotropic hardening effect after plastic pre-deformation by means of monotonic tension up to 5 % and 15 % axial strain (Dietrich and Kowalewski, 1997), whereas CP-Ti exhibited kinematic hardening for 1 % tensile pre-deformation (Dubey et al., 2023), which is similar to the reported kinematic hardening effect observed in the Ti-Cu bimetal after

Table 3
The fitting errors associated with the yield surfaces for Ti-Cu bimetal in the as-received state and after subsequent pre-deformation resulting from monotonic tension, as well as combined monotonic tension with cyclic torsion of strain amplitude equal to: ± 0.1 % and ± 0.15 % at frequency of: 0.5 Hz and 1 Hz.

As-received	Monotonic tension deformed	±0.1 % at 0.5 Hz deformed	±0.15 % at 0.5 Hz deformed	±0.1 % at 1 Hz deformed	±0.15 % at 1 Hz deformed
6.69E-02	1.06E-01	2.43E-01	1.93E-01	2.84E-01	1.78E-01

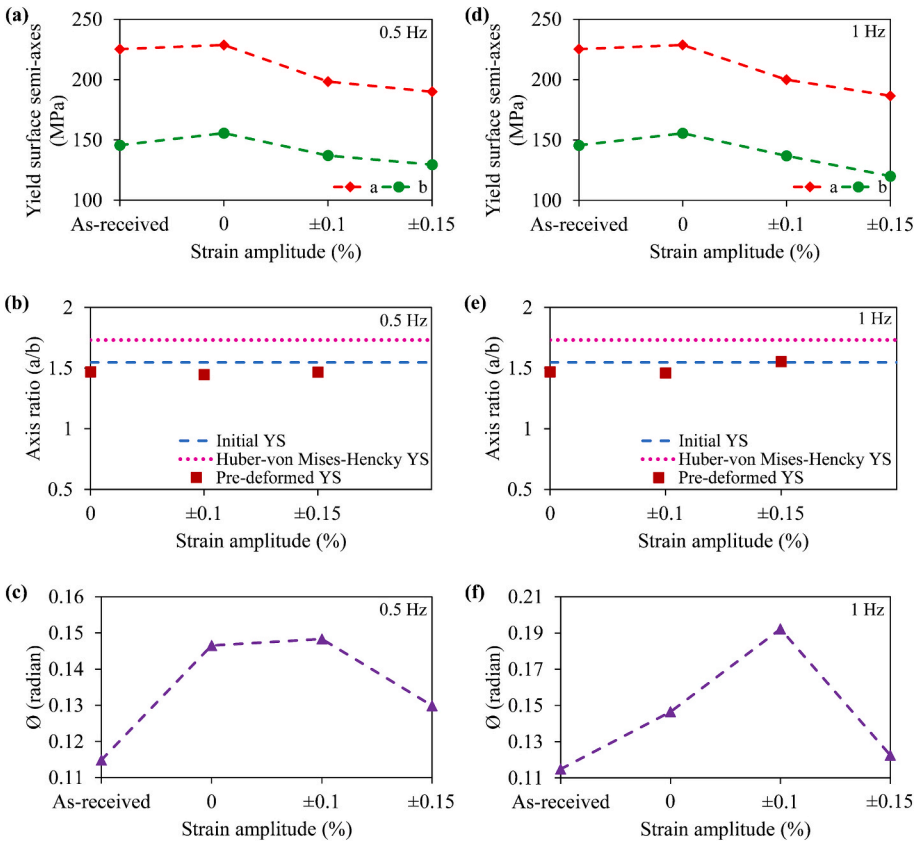

Fig. 12. Variation of the yield surface parameters of Ti-Cu bimetal due to pre-deformation by monotonic tension (0 % strain amplitude); combined monotonic tension with cyclic torsion of strain amplitude equal to: ±0.1 % and ± 0.15 % at frequency of: 0.5 Hz (a, b, c) and 1 Hz (d, e, f), respectively.

1 % monotonic plastic pre-deformation. In the case of plastic pre-deformation caused by monotonic tension assisted by cyclic torsion, CP-Cu and CP-Ti showed hardening in tensile yield stress direction and softening in all other stress directions for strain amplitudes varying from ± 0.2 % to ± 0.7 % (Dubey et al., 2023; Kowalewski et al., 2014). Conversely, the reported Ti-Cu bimetal exhibited a softening effect in all biaxial stress directions under similar loading conditions.

These findings emphasize the importance of doing experimental analysis to comprehend the plastic behaviour of bimetals, as it cannot be solely predicted based on the behaviour of their constituent metals. The plastic behaviour of bimetals is extensively controlled by parameters such as the bonding quality, thickness of each metal and variations in microstructure at the interfaces of both metals.

3.6. Microstructural characteristics of the Ti-Cu bimetal in the as-received state and after loading history induced

EBSD results at solid–solid bonded Ti-Cu interface were presented in Figs. 14 and 15. The figures reveal the nature of grain structure and texture evolution in the form of Inverse Pole Figure (IPF) maps, as well as (001) and (0001) pole figures in the as-received state of bimetal and after its deformation. The planes with the three typical miller indices {001}, {101}, {111} for copper, and {0001}, $\{2\bar{1}\bar{1}0\}$, $\{10\bar{1}0\}$ for titanium were displayed in RGB (red, green and blue) colours, respectively. Each map was related to the specific yield surface presented in Fig. 13. All specimens were fully recrystallized after the plastic pre-deformation.

The microstructure of the as-received bimetal was characterized by the finer grains near interface and coarse structure far from it in copper, embedded with many twins. More or less equal sized grains with a high number of deformation twins were found in titanium, as presented in Fig. 14a. Additionally, the fine equiaxed grains were observed at the interface zone, which was in a span of average 7–8 μm width. The size of the grains was uniform in the deformed Ti-Cu interface (Fig. 14a). By comparing the grain maps of the as-received state (Fig. 14a) and 1 % tensile pre-deformed state (Fig. 14b), it was evident, that tensile pre-deformation leads to a refined grain size with elongated grains along the tensile loading direction in copper. Also, the copper grains were more deformed and merged with the interface. The width of Ti-Cu bimetal interface increased up to the average value of 34 μm (Fig. 14b). The fine grain structure implies, that severe plastic deformation creates more nucleating sites that leads to the grain refinement. When bimetal was deformed under combined tension-cyclic torsion (Fig. 14c, d, e, f), the average grain size of copper increased with the increase of strain amplitude and frequency in comparison to the prior deformation due to tension, only (Fig. 14b). The grain map (Fig. 14e) demonstrates that the pre-deformation caused by combined monotonic tension-cyclic torsion with ± 0.1 % strain amplitude at frequency equal to 1 Hz enlarges the grain size of copper and elongates the grains in a spoke-wise pattern. The interface zone in bimetal deformed due to combination of tension assisted by cyclic torsion with ± 0.1 % strain amplitude at 0.5 Hz frequency (Fig. 14c) decreased in comparison to the bimetal deformed due to tension, only (Fig. 14b). However, with the increase of strain amplitude and frequency, an opposite effect can be observed, i.e. the width of the interface zone increased. One can also observe, that with the increase of cyclic shear strain amplitude from ± 0.1 % (Fig. 14c) to ± 0.15 % (Fig. 14d) at the frequency equal to 0.5 Hz, the size of grains at the interface transformed from fine to ultrafine. Similar trend can also be observed at the higher frequency equal to 1 Hz (Fig. 14e, 14f). In the case of titanium, more or less similar average grain sizes were obtained for all bimetal states considered. It means, that all types of pre-deformation applied do not affect significantly the grain structure of titanium. Such behaviour was also reported in previous work for the experimental program performed under higher magnitudes of prior deformation (Dubey et al., 2023).

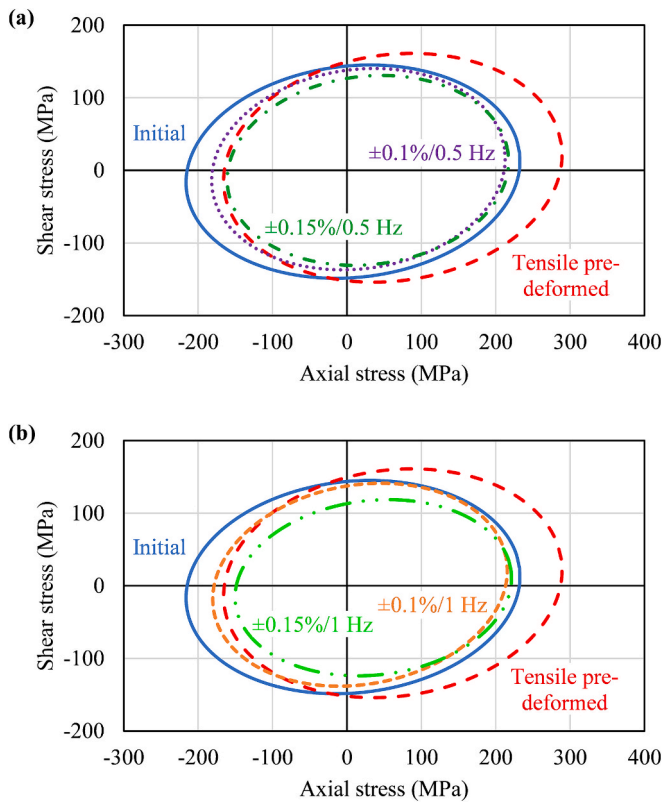

Fig. 13. Evolution of the initial yield surface of Ti-Cu bimetal due to pre-deformation caused by monotonic tension; monotonic tension assisted by cyclic torsion with strain amplitudes of ± 0.1 % and ± 0.15 % at frequency values equal to 0.5 Hz (a) and 1 Hz (b), respectively.

When examining the deformation characteristics of the Ti-Cu bimetallic interface, it is evident that increasing the amplitude of cyclic shear strain from ± 0.1 % (Fig. 14c) to ± 0.15 % (Fig. 14d) at a frequency of 0.5 Hz results in a greater amount of recrystallization at the interface. This, in turn, leads to a greater degree of material softening reflected by adequate sizes of the yield surface. This phenomenon becomes more pronounced as the frequency is further increased from 0.5 Hz to 1 Hz (Fig. 14e, 14f).

As it can be seen from the (001) pole figures in Fig. 15, the copper has a nearly random texture in all states. More interestingly, a texture or crystallographic orientation of copper near the interface was dominant in < 101 > and < 111 > directions (Fig. 14), that can be also observed in Fig. 15, as the high intensity points located in those areas of the pole figures were found. In the case of combined tension-cyclic torsion with ± 0.1 % strain amplitude at frequencies equal to 0.5 Hz (Fig. 15c) and 1 Hz (Fig. 15e), the closed-packed < 001 > direction was also distinguished. Evolution of the titanium crystallographic textures recorded on basal plane (0001) in the extrusion plane (ED-RD) was presented in Fig. 15. The pole figure of titanium (0001) near the interface illustrates the RD split basal texture for the bimetal in the as-received state (Fig. 15a). The basal texture with c-axis of the majority of grains is inclined at an angle of ± (20° – 60°) from the TD towards the RD. More interestingly, the texture shows, that the c-axis of grains near the interface are preferentially oriented perpendicularly to the extrusion direction. Fig. 15b represents the pole figures after the 1 % tensile pre-deformation. It reveals a development of the RD split basal texture with the c-axes widely distributed in the whole RD-TD plane, since a line in the pole figure represents the plane. However, a weaker texture component with the c-axes oriented almost in parallel to the ED appeared as well. When bimetal was deformed by combined monotonic tension assisted by cyclic torsion with ± 0.1 % strain amplitude at 0.5 Hz frequency (Fig. 15c), two stronger basal textures were observed; first one with the c-axes inclined at (40° – 80°) from the TD towards the RD and the second one with the c-axes in parallel to the TD. Also, some weaker basal texture aligned in parallel to the – RD and ED still occurred in the microstructure. However, with the increase of strain amplitude from ± 0.1 % to ± 0.15 % at 0.5 Hz frequency (Fig. 15d), the weaker texture component parallel to the ED disappeared and the RD split basal texture with most of the grains reoriented their c-axis in parallel to the RD. One could notice a stronger basal texture with the c-axes aligned in parallel to the ± RD and TD; weaker basal texture distributed non-uniformly in the plane parallel to the ED-RD plane when the pre-deformation was induced by combined tension and cyclic torsion with ± 0.1 % strain amplitude at 1 Hz frequency (Fig. 15e). Based on the pole figure of material after the ± 0.15 % cyclic strain amplitude at the frequency equal to 1 Hz (Fig. 15f), the basal texture was observed for 3 different high-intensity orientations. First, with narrow distribution of the c-axes inclined at (20° – 50°) from the TD towards the positive ED-RD plane; second, with the c-axes inclined at (50° – 60°) from the TD towards negative RD, and third, with the c-axes inclined at (64° – 78°) from the TD towards ED – (−RD) plane.

The texture intensities are represented by the colour scale bar corresponding to each pole figures. It is evident from the pole figures in Fig. 15, that the intensity value is considerably lower for the bimetal deformed by monotonic tension (Fig. 15b) in comparison to the same material in the as-received state (Fig. 15a). This is attributed to localized grain elongation and interface zone widening in copper, triggered by the applied tensile pre-deformation. However, when bimetal was deformed due to combination of the monotonic tension and cyclic torsion, the intensity gradually increased in copper with the increase of strain amplitudes at both values of frequency taken into account. It reached a maximum of 12.6 in the case of material subjected to tension assisted by cyclic torsion with ± 0.15 % strain amplitude at frequency equal to 1 Hz (Fig. 15f). An opposite trend can be observed in titanium for which the peak intensity value equal to 19.9 was obtained for ± 0.1 % strain amplitude at frequency of 1 Hz (Fig. 15e). Such increase in intensity value indicates a development of the stable orientation after combined pre-deformation towards (001) and (0001) crystallographic planes of the Ti-Cu bimetal specimens in the extrusion plane (ED-RD).

The plastic pre-deformation process (1 % tension and ± 0.1–0.15 % cyclic shear) of Ti-Cu bimetal leads to a notable texture evolution, especially in the copper side and at the Ti-Cu interface. This is attributed to strain localization, recrystallization effects, and cumulative shear under cyclic loading. The evolution is more pronounced in copper due to its higher susceptibility to crystallographic reorientation under deformation, while titanium showed more stable textures with subtle reorganization. The internal misorientation within the grains is also evident through the colour variations in individual grain interior. It is worth to note, that after loading histories applied to pre-deform the bimetal tested, the interfaces of Ti-Cu were still intact. These results clearly support an evolution of the initial yield surface of bimetal due to prior deformation illustrated in Fig. 13.

4. Conclusions

In this research, a pioneer investigation of the evolution of initial yield surface reflecting plastic pre-deformation of the Ti-Cu bimetal were performed. An experimental procedure was selected to investigate the effect of monotonic tension and combined tension-cyclic torsion pre-deformation on the mechanical properties of the bimetal. Initial and subsequent yield loci of the Ti-Cu bimetal were systematically investigated after various pre-deformation levels using the single specimen approach with 0.01 % plastic offset strain as definition of yield point. The main findings can be summarized as follows:

- The mechanical properties of bimetal lie in between those of its constituent metals. The tensile yield and ultimate strengths were

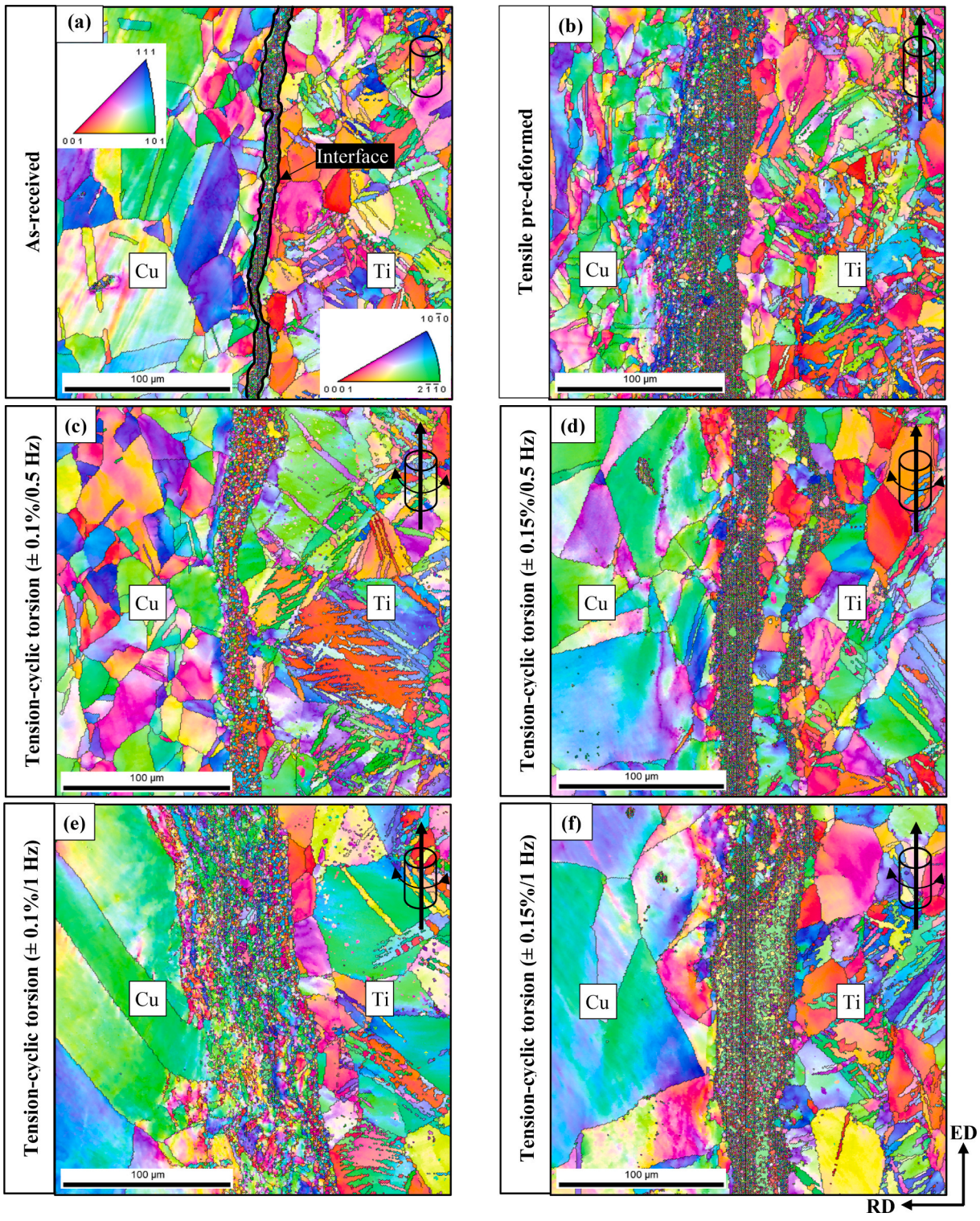

Fig. 14. Inverse pole figure (IPF) maps of the as-received material (a); after monotonic tension to 1 % (b); monotonic tension assisted by cyclic torsion of strain amplitudes equal to ± 0.1 % (c) and ± 0.15 % (d) at frequency equal to 0.5 Hz; and ± 0.1 % (e) and ± 0.15 % (f) at frequency equal to 1 Hz.

approximately 43 % and 50 % higher than those of copper, respectively.

- Cyclic torsion applied during monotonic tension caused a significant decrease of tensile stress. The tensile stress reduction becomes greater with an increase of torsional strain amplitude and frequency.
- The initial yield surface of the as-received Ti-Cu bimetal exhibited anisotropy, which was clearly identified by its comparison to the Huber – von Mises – Hencky isotropic yield surface. A tension–compression asymmetry can be easily observed on the initial yield surface.
- Kinematic hardening effect was identified for the pre-strained bimetal on the basis of subsequent yield surface following 1 % monotonic tensile pre-deformation in comparison to the as-received state, whereas, kinematic softening was found after the combined pre-deformation due to monotonic tension assisted by cyclic torsion.

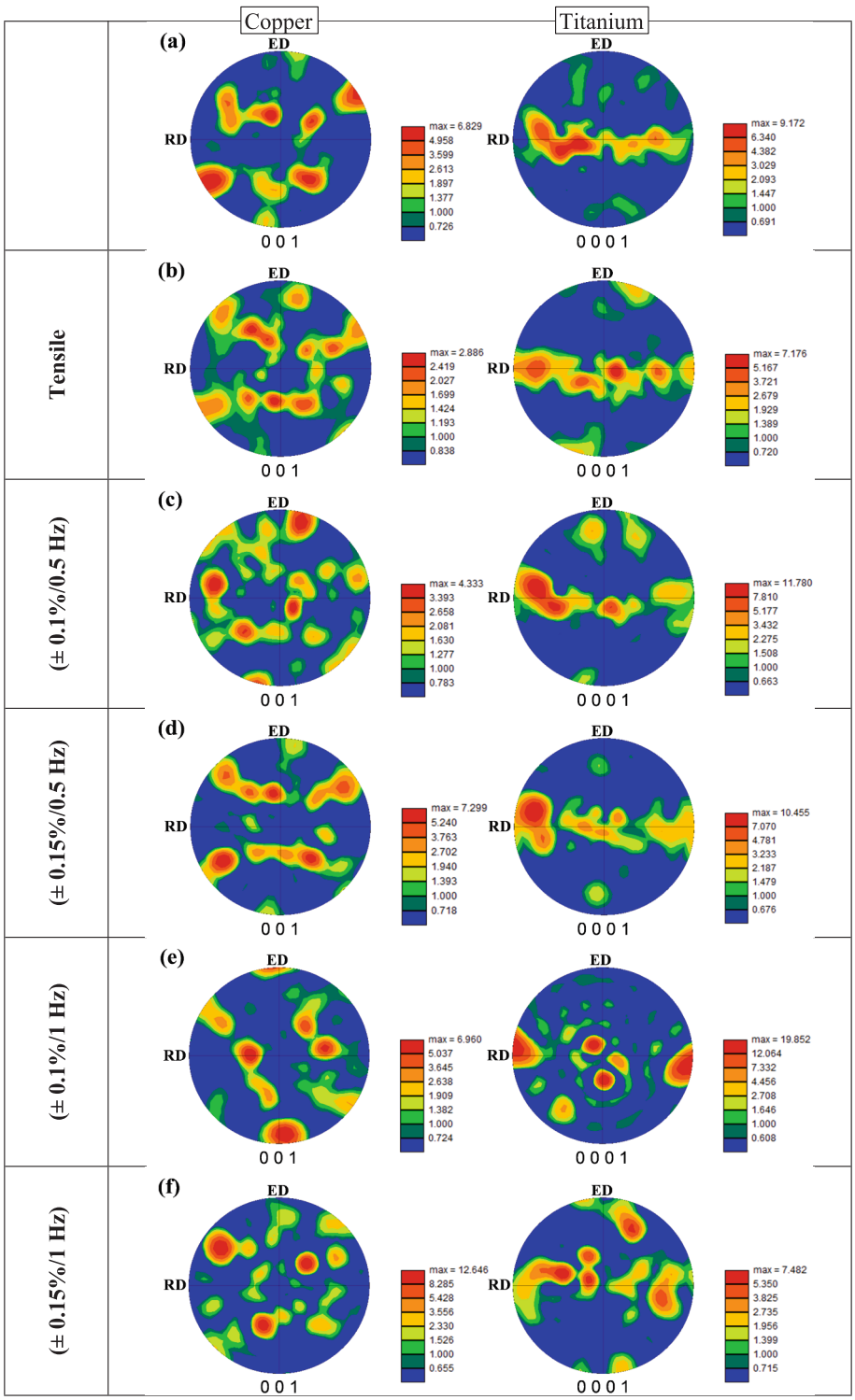

Fig. 15. Pole figure maps of the as-received material (a); after monotonic tension to 1 % (b); monotonic tension assisted by cyclic torsion of strain amplitudes equal to ± 0.1 % (c) and ± 0.15 % (d) at frequency equal to 0.5 Hz; and ± 0.1 % (e) and ± 0.15 % (f) at frequency equal to 1 Hz.

Effect of kinematic softening became more prominent with the increase of cyclic torsion strain amplitude and frequency.

- EBSD analysis performed on the pre-deformed specimens revealed, that only shear strain magnitude of the combined pre-deformation condition affects the yielding behaviour of bimetallic structure. The higher strain magnitude is leading to notable microstructural changes involving activation of more slip systems which in turn cause material recrystallization and subsequent softening in the radial direction.

CRediT authorship contribution statement

Ved Prakash Dubey: Writing – original draft, Visualization, Software, Methodology, Investigation, Formal analysis, Data curation. **Mateusz Kopec:** Writing – review & editing, Writing – original draft,

Visualization, Validation, Supervision, Software, Resources, Project administration, Methodology, Investigation, Funding acquisition, Formal analysis, Data curation, Conceptualization. **Magdalena Łazińska:** Methodology, Investigation. **Zbigniew L. Kowalewski:** Writing – review & editing, Validation, Supervision, Funding acquisition, Formal analysis, Conceptualization.

Declaration of competing interest

The authors declare that they have no known competing financial interests or personal relationships that could have appeared to influence the work reported in this paper.

Acknowledgements

The authors would like to express their gratitude to the technical staff – Mr M. Wyszkowski and Mr A. Chojnacki for their kind help during the experimental part of this work and Dr Dariusz Zasada from Military University of Technology for his support during EBSD measurements.

This work has been supported by the National Science Centre through the Grant No 2019/35/B/ST8/03151.

Appendix A:. Derivation of equivalent strain (ε_{eq}) formulation

In plasticity theory, the equivalent (or effective) strain is defined to ensure that the plastic work per unit volume is equivalent whether computed from the full stress–strain tensors or from scalar invariants:

$$dw^p = \sigma_{ij} d\varepsilon_{ij}^p = \sigma_{eq} d\varepsilon_{eq}^p \tag{A1}$$

This leads to a definition of the equivalent strain based on the second invariant of the deviatoric strain tensor:

$$\varepsilon_{eq} = \sqrt{\frac{2}{3}\varepsilon_{ij}^{'}\varepsilon_{ij}^{'}} \tag{A2}$$

where, $\varepsilon_{ij}^{'}$ is the deviatoric strain tensor, defined as:

$$\varepsilon_{ij}^{'} = \varepsilon_{ij} - \frac{1}{3}\delta_{ij}\varepsilon_{kk} \tag{A3}$$

and its components can be expressed as:

$$\begin{aligned}
\varepsilon_{xx}^{'} &= \varepsilon_{xx} - \frac{1}{3}(\varepsilon_{xx} + \varepsilon_{yy} + \varepsilon_{zz}) \\
\varepsilon_{yy}^{'} &= \varepsilon_{yy} - \frac{1}{3}(\varepsilon_{xx} + \varepsilon_{yy} + \varepsilon_{zz}) \\
\varepsilon_{zz}^{'} &= \varepsilon_{zz} - \frac{1}{3}(\varepsilon_{xx} + \varepsilon_{yy} + \varepsilon_{zz}) \\
\varepsilon_{xy}^{'} &= \varepsilon_{xy} \\
\varepsilon_{yz}^{'} &= \varepsilon_{yz} \\
\varepsilon_{zx}^{'} &= \varepsilon_{zx}
\end{aligned} \tag{A4}$$

Using the above expression of normal deviatoric strain components, the following form can be expressed:

$$\left(\varepsilon_{xx}^{'2} + \varepsilon_{yy}^{'2} + \varepsilon_{zz}^{'2}\right) = \frac{1}{3}\left[(\varepsilon_{xx} - \varepsilon_{yy})^2 + (\varepsilon_{yy} - \varepsilon_{zz})^2 + (\varepsilon_{zz} - \varepsilon_{xx})^2\right] \tag{A5}$$

Now solving for the equivalent strain:

$$\varepsilon_{eq} = \sqrt{\frac{2}{3}\varepsilon_{ij}^{'}\varepsilon_{ij}^{'}} = \sqrt{\frac{2}{3}\left[\left(\varepsilon_{xx}^{'2} + \varepsilon_{yy}^{'2} + \varepsilon_{zz}^{'2}\right) + 2\left(\varepsilon_{xy}^{'2} + \varepsilon_{yz}^{'2} + \varepsilon_{zx}^{'2}\right)\right]} \tag{A6}$$

replacing the deviatoric strain components:

$$\varepsilon_{eq} = \sqrt{\frac{2}{3}\left[\frac{1}{3}\left((\varepsilon_{xx} - \varepsilon_{yy})^2 + (\varepsilon_{yy} - \varepsilon_{zz})^2 + (\varepsilon_{zz} - \varepsilon_{xx})^2\right) + 2\left(\varepsilon_{xy}^2 + \varepsilon_{yz}^2 + \varepsilon_{zx}^2\right)\right]} \tag{A7}$$

after simplifying:

$$\varepsilon_{eq} = \frac{\sqrt{2}}{3}\sqrt{(\varepsilon_{xx} - \varepsilon_{yy})^2 + (\varepsilon_{yy} - \varepsilon_{zz})^2 + (\varepsilon_{zz} - \varepsilon_{xx})^2 + 6\left(\varepsilon_{xy}^2 + \varepsilon_{yz}^2 + \varepsilon_{zx}^2\right)} \tag{A8}$$

The above equation (A.8) is known as classical von Mises equivalent strain expression in plasticity theory when material is assumed to behave as perfectly incompressible (i.e. when $\nu = 0.5$). But no real-world material is perfectly incompressible.

Therefore, to account for material compressibility, the above expression is scaled by incorporating a material constant (Poisson's ratio, ν) and is expressed as:

$$\varepsilon_{eq} = \frac{\sqrt{2}}{2(1+\nu)}\sqrt{(\varepsilon_{xx}-\varepsilon_{yy})^2+(\varepsilon_{yy}-\varepsilon_{zz})^2+(\varepsilon_{zz}-\varepsilon_{xx})^2+6\left(\varepsilon_{xy}^2+\varepsilon_{yz}^2+\varepsilon_{zx}^2\right)} \tag{A9}$$

This scaling ensures the strain energy from the scalar equivalent strain matches that from the tensor formulation in elastic regime, and works for plasticity modelling when using the von Mises yield function. This expression is valid for materials with different compressibility behaviour.

When a uniaxial stress is applied in the x direction for an isotropic material, the transverse strains are $\varepsilon_{yy} = \varepsilon_{zz} = -\nu\varepsilon_{xx}$, and shear strains are equal to zero. Thus for a uniaxial stress state:

$$\varepsilon_{eq} = \frac{\sqrt{2}}{2(1+\nu)}\sqrt{(\varepsilon_{xx}+\nu\varepsilon_{xx})^2+(-\nu\varepsilon_{xx}-\varepsilon_{xx})^2} = \frac{\sqrt{2}}{2(1+\nu)}\sqrt{2(1+\nu)^2\varepsilon_{xx}^2} = \varepsilon_{xx} \tag{10}$$

For a state of pure torsional loading:

$$\varepsilon_{eq} = \frac{\sqrt{2}}{2(1+\nu)}\sqrt{6(\varepsilon_{xy})^2} = \frac{\sqrt{3}}{(1+\nu)}\varepsilon_{xy} \tag{11}$$

Therefore, for a combined state of uniaxial tension and torsion loading:

$$\varepsilon_{eq} = \sqrt{\varepsilon_{xx}^2+\frac{3}{(1+\nu)^2}\varepsilon_{xy}^2} \tag{12}$$

This final form (Equation (A.12)) remains consistent with the energy equivalence principle and is appropriate for interpreting the multiaxial (axial + torsional loading) strain states observed in this study.

Data availability

Data will be made available on request.

References

Beygi, R., Mehrizi, M.Z., Verdera, D., Loureiro, A., 2018. Influence of tool geometry on material flow and mechanical properties of friction stir welded Al-Cu bimetals. J. Mater. Process. Technol. 255, 739–748. https://doi.org/10.1016/j.jmatprotec.2018.01.033.

Chen, Y., Zuo, X., Zhang, W., Hao, Z., Li, Y., Luo, Z., Ao, S., 2022. Enhanced strength-ductility synergy of bimetallic laminated steel structure of 304 stainless steel and low-carbon steel fabricated by wire and arc additive manufacturing. Mater. Sci. Eng. A 856, 143984. https://doi.org/10.1016/j.msea.2022.143984.

Dietrich, L., Kowalewski, Z.L., 1997. Experimental investigation of an anisotropy in copper subjected to predeformation due to constant and monotonic loadings. Int. J. Plast 13, 87–109. https://doi.org/10.1016/S0749-6419(97)00002-8.

Dietrich, L., Socha, G., 2012. Accumulation of damage in A336 GR5 Structural Steel Subject to complex stress Loading. Strain 48, 279–285. https://doi.org/10.1111/j.1475-1305.2011.00821.x.

Du, K., Huang, S., Hou, Y., Wang, H., Wang, Y., Zheng, W., Yuan, X., 2023. Characterization of the asymmetric evolving yield and flow of 6016-T4 aluminum alloy and DP490 steel. Journal of Materials Science & Technology 133, 209–229. https://doi.org/10.1016/j.jmst.2022.05.040.

Dubey, V.P., Kopec, M., Łazińska, M., Kowalewski, Z.L., 2023. Yield surface identification of CP-Ti and its evolution reflecting pre-deformation under complex loading. Int. J. Plast 167, 103677. https://doi.org/10.1016/j.ijplas.2023.103677.

Findik, F., 2011. Recent developments in explosive welding. Mater. Des. 32, 1081–1093. https://doi.org/10.1016/j.matdes.2010.10.017.

Gao, X., Jiang, Z., Wei, D., Jiao, S., Chen, D., Xu, J., Zhang, X., Gong, D., 2014. Effects of temperature and strain rate on microstructure and mechanical properties of high chromium cast iron/low carbon steel bimetal prepared by hot diffusion-compression bonding. Mater. Des. 63, 650–657. https://doi.org/10.1016/j.matdes.2014.06.067.

Ghosh, M., Chatterjee, S., 2005. Effect of interface microstructure on the bond strength of the diffusion welded joints between titanium and stainless steel. Mater Charact 54, 327–337. https://doi.org/10.1016/j.matchar.2004.12.007.

Gil, C.M., Lissenden, C.J., Lerch, B.A., 1999. Yield of Inconel 718 by Axial-Torsional Loading at Temperatures up to 649°C. J. Test. Eval. 27, 327–336. https://doi.org/10.1520/jte12233j.

Gotawala, N., Shrivastava, A., 2021. Investigation of interface microstructure and mechanical properties of rotatory friction welded dissimilar aluminum-steel joints. Mater. Sci. Eng. A 825, 141900. https://doi.org/10.1016/j.msea.2021.141900.

Hecker, S.S., 1971. Yield surfaces in prestrained aluminum and copper. Metall Trans 2, 2077–2086. https://doi.org/10.1007/BF02917534.

Helling, D.E., Miller, A.K., Stout, M.G., 1986. An Experimental Investigation of the Yield Loci of 1100-0 Aluminum, 70:30 Brass, and an Overaged 2024 Aluminum Alloy after Various Prestrains. J. Eng. Mater. Technol. 108, 313–320. https://doi.org/10.1115/1.3225888.

Hencky, H., 1924. Zur Theorie plastischer Deformationen und der hierdurch im Material hervorgerufenen Nachspannungen. ZAMM - Journal of Applied Mathematics and Mechanics / Zeitschrift Für Angewandte Mathematik Und Mechanik 4, 323–334. https://doi.org/10.1002/zamm.19240040405.

Hong, H.K., Liu, L.W., Shiao, Y.P., Yan, S.F., 2022. Yield Surface Evolution and Elastoplastic Model with Cubic Distortional Yield Surface. J. Eng. Mech. 148, 04022027. https://doi.org/10.1061/(ASCE)EM.1943-7889.0002108.

Hou, Y., Min, J., Guo, N., Lin, J., Carsley, J.E., Stoughton, T.B., Traphöner, H., Clausmeyer, T., Tekkaya, A.E., 2021. Investigation of evolving yield surfaces of dual-phase steels. Journal of Materials Processing Technology, Professor Marciniak 100th Birthday Special Issue on Metal Forming 287, 116314. https://doi.org/10.1016/j.jmatprotec.2019.116314.

Hu, G., Zhang, K., Huang, S., Ju, J.W.W., 2012. Yield surfaces and plastic flow of 45 steel under tension-torsion loading paths. Acta Mech. Solida Sin. 25, 348–360. https://doi.org/10.1016/S0894-9166(12)60032-9.

Huber, M.T., 1904. Specific work of deformation as a measure of material effort (in polish: Właściwa praca odkształcenia jako miara wytężenia materyału). Towarzystwo Politechniczne.

Iftikhar, C.M.A., Brahme, A., Inal, K., Khan, A.S., 2022. An evolution of subsequent yield loci under proportional and non-proportional loading path of 'as-received' extruded AZ31 magnesium alloy: Experiments and CPFEM modeling. Int. J. Plast 151, 103216. https://doi.org/10.1016/j.ijplas.2022.103216.

Iftikhar, C.M.A., Li, Y.L., Kohar, C.P., Inal, K., Khan, A.S., 2021. Evolution of subsequent yield surfaces with plastic deformation along proportional and non-proportional loading paths on annealed AA6061 alloy: Experiments and crystal plasticity finite element modeling. Int. J. Plast 143, 102956. https://doi.org/10.1016/j.ijplas.2021.102956.

Ishikawa, H., 1997. Subsequent yield surface probed from its current center. Int. J. Plast 13, 533–549. https://doi.org/10.1016/S0749-6419(97)00024-7.

Ivey, H.J., 1961. Plastic Stress–Strain Relations and Yield Surfaces for Aluminium Alloys. J. Mech. Eng. Sci. 3, 15–31. https://doi.org/10.1243/JMES_JOUR_1961_003_005_02.

Kabirian, F., Khan, A.S., 2015. Anisotropic yield criteria in σ–τ stress space for materials with yield asymmetry. Int. J. Solids Struct. 67–68, 116–126. https://doi.org/10.1016/j.ijsolstr.2015.04.006.

Khan, A.S., Kazmi, R., Pandey, A., Stoughton, T., 2009. Evolution of subsequent yield surfaces and elastic constants with finite plastic deformation. Part-I: a very low work hardening aluminum alloy (Al6061-T6511). International Journal of Plasticity, Exploring New Horizons of Metal Forming Research 25, 1611–1625. https://doi.org/10.1016/j.ijplas.2008.07.003.

Khan, A.S., Pandey, A., Stoughton, T., 2010. Evolution of subsequent yield surfaces and elastic constants with finite plastic deformation. Part II: a very high work hardening aluminum alloy (annealed 1100 Al). Int. J. Plast 26, 1421–1431. https://doi.org/10.1016/j.ijplas.2009.07.008.

Khan, A.S., Wang, X., 1993. An experimental study on subsequent yield surface after finite shear prestraining. Int. J. Plast 9, 889–905. https://doi.org/10.1016/0749-6419(93)90056-V.

Kim, K.H., 1992. Evolution of anisotropy during twisting of cold drawn tubes. J. Mech. Phys. Solids 40, 127–139. https://doi.org/10.1016/0022-5096(92)90282-7.

Kimura, M., Iijima, T., Kusaka, M., Kaizu, K., Fuji, A., 2016. Joining phenomena and tensile strength of friction welded joint between Ti–6Al–4V titanium alloy and low carbon steel. J. Manuf. Process. 24, 203–211. https://doi.org/10.1016/j.jmapro.2016.09.004.

Kowalewski, Z.L., Śliwowski, M., 1997. Effect of cyclic loading on the yield surface evolution of 18G2A low-alloy steel. Int. J. Mech. Sci. 39, 51–68. https://doi.org/10.1016/0020-7403(96)00016-1.

Kowalewski, Z.L., Szymczak, T., Maciejewski, J., 2014. Material effects during monotonic-cyclic loading. Int. J. Solids Struct. 51, 740–753. https://doi.org/10.1016/j.ijsolstr.2013.10.040.

Kowalewski, Z.L., Turski, K., 2003. Multiaxial Proportional and Non-Proportional Cyclic Behaviour of 40H Steel and PA6 Aluminium Alloy. Key Eng. Mater. 233–236, 269–274. https://doi.org/10.4028/www.scientific.net/KEM.233-236.269.

Lee, J.S., Son, H.T., Oh, I.H., Kang, C.S., Yun, C.H., Lim, S.C., Kwon, H.C., 2007. Fabrication and characterization of Ti–Cu clad materials by indirect extrusion. Journal of Materials Processing Technology, 3rd International Conference on Advanced Forming and Die Manufacturing Technology 187–188, 653–656. https://doi.org/10.1016/j.jmatprotec.2006.11.144.

Lee, W., Chung, K.H., Kim, D., Kim, J., Kim, C., Okamoto, K., Wagoner, R.H., Chung, K., 2009. Experimental and numerical study on formability of friction stir welded TWB sheets based on hemispherical dome stretch tests. International Journal of Plasticity, Exploring New Horizons of Metal Forming Research 25, 1626–1654. https://doi.org/10.1016/j.ijplas.2008.08.005.

Liu, C., Yang, X., Ding, Y., Li, H., Wan, S., Guo, Y., Li, Y., 2023. The yielding behavior of TU00 pure copper under impact loading. Int. J. Mech. Sci. 245, 108110. https://doi.org/10.1016/j.ijmecsci.2023.108110.

Liu, G.L., Huang, S.H., Shi, C.S., Zeng, B., Zhang, K.S., Zhong, X.C., 2018. Experimental Investigations on subsequent Yield Surface of Pure Copper by Single-Sample and Multi-Sample Methods under Various Pre-Deformation. Materials 11, 277. https://doi.org/10.3390/ma11020277.

Lu, D., Zhang, K., Hu, G., Lan, Y., Chang, Y., 2020. Investigation of Yield Surfaces Evolution for Polycrystalline Aluminum after Pre-Cyclic Loading by Experiment and Crystal Plasticity simulation. Materials 13, 3069. https://doi.org/10.3390/ma13143069.

Mair, W.M., Pugh, H.L.D., 1964. Effect of Pre-Strain on Yield Surfaces in copper. J. Mech. Eng. Sci. 6, 150–163. https://doi.org/10.1243/JMES_JOUR_1964_006_025_02.

Matsushita, T., Noguchi, M., Arimura, K., 1988. Hot hydrostatic extrusion of Ti/Cu-alloy composite materials. J. Soc. Mater. Sci. Jpn 37, 107–113. https://doi.org/10.2472/jsms.37.107.

Miastkowski, J., Szczepiński, W., 1965. An experimental study of yield surfaces of prestrained brass. Int. J. Solids Struct. 1, 189–194. https://doi.org/10.1016/0020-7683(65)90026-0.

Mises, R.V., 1913. Mechanik der festen Körper im plastisch- deformablen Zustand. Nachrichten Von Der Gesellschaft Der Wissenschaften Zu Göttingen, Mathematisch-Physikalische Klasse 1913, 582–592.

Naghdi, P.M., Essenburg, F., Koff, W., 1958. An Experimental Study of initial and subsequent Yield Surfaces in Plasticity. J. Appl. Mech. 25, 201–209. https://doi.org/10.1115/1.4011745.

Naka, T., Uemori, T., Hino, R., Kohzu, M., Higashi, K., Yoshida, F., 2008. Effects of strain rate, temperature and sheet thickness on yield locus of AZ31 magnesium alloy sheet. Journal of Materials Processing Technology, 10th International Conference on Advances in Materials and Processing Technologies 201, 395–400. https://doi.org/10.1016/j.jmatprotec.2007.11.189.

Onuike, B., Bandyopadhyay, A., 2019. Bond strength measurement for additively manufactured Inconel 718- GRCop84 copper alloy bimetallic joints. Addit. Manuf. 27, 576–585. https://doi.org/10.1016/j.addma.2019.04.003.

Phillips, A., Das, P.K., 1985. Yield surfaces and loading surfaces of aluminum and brass: an experimental investigation at room and elevated temperatures. Int. J. Plast 1, 89–109. https://doi.org/10.1016/0749-6419(85)90015-4.

Phillips, A., Juh-Ling, T., 1972. The effect of loading path on the yield surface at elevated temperatures. Int. J. Solids Struct. 8, 463–474. https://doi.org/10.1016/0020-7683(72)90017-0.

Sahasrabudhe, H., Harrison, R., Carpenter, C., Bandyopadhyay, A., 2015. Stainless steel to titanium bimetallic structure using LENS^{TM}. Addit. Manuf. 5, 1–8. https://doi.org/10.1016/j.addma.2014.10.002.

Shi, B., Peng, Y., Yang, C., Pan, F., Cheng, R., Peng, Q., 2017. Loading path dependent distortional hardening of Mg alloys: Experimental investigation and constitutive modeling. Int. J. Plast 90, 76–95. https://doi.org/10.1016/j.ijplas.2016.12.006.

Shiratori, E., Ikegami, K., Kaneko, K., 1973. The Influence of the Bauschinger effect on the subsequent Yield Condition. Bulletin of JSME 16, 1482–1493. https://doi.org/10.1299/jsme1958.16.1482.

Shiratori, E., Ikegami, K., Yoshida, F., Kaneko, K., Koike, S., 1976. The subsequent Yield Surfaces after Preloading under combined Axial load and Torsion. Bulletin of JSME 19, 877–883. https://doi.org/10.1299/jsme1958.19.877.

Štefan, J., Parma, S., Marek, R., Plešek, J., Ciocanel, C., Feigenbaum, H., 2021. Overview of an Experimental Program for Development of Yield Surfaces Tracing Method. Appl. Sci. 11, 7606. https://doi.org/10.3390/app11167606.

Stout, M.G., Martin, P.L., Helling, D.E., Canova, G.R., 1985. Multiaxial yield behavior of 1100 aluminum following various magnitudes of prestrain. Int. J. Plast 1, 163–174. https://doi.org/10.1016/0749-6419(85)90027-0.

Sung, S.J., Liu, L.W., Hong, H.K., Wu, H.C., 2011. Evolution of yield surface in the 2D and 3D stress spaces. Int. J. Solids Struct. 48, 1054–1069. https://doi.org/10.1016/j.ijsolstr.2010.12.011.

Szczepinski, W., 1993. On deformation-induced plastic anisotropy of sheet metals. Arch. Mech. 45, 3–38.

Tan, C., Zhou, K., Ma, W., Min, L., 2018. Interfacial characteristic and mechanical performance of maraging steel-copper functional bimetal produced by selective laser melting based hybrid manufacture. Mater. Des. 155, 77–85. https://doi.org/10.1016/j.matdes.2018.05.064.

Uścinowicz, R., 2022. Effect of Elevated Temperature and Annealing Time on Mechanical Properties of Ti/Cu Bimetal. Materials 15, 8707. https://doi.org/10.3390/ma15238707.

Uscinowicz, R., 2013. Experimental identification of yield surface of Al–Cu bimetallic sheet. Compos. B Eng. 55, 96–108. https://doi.org/10.1016/j.compositesb.2013.06.002.

Volokitina, I., Naizabekov, A.B., Volokitin, A.V., 2023a. Effect of Deformation by Ecap-drawing Method on Change in Steel-Aluminum Wire Properties. Metallurgist 66, 1235–1240. https://doi.org/10.1007/s11015-023-01436-0.

Volokitina, I., Sapargaliyeva, B., Agabekova, A., Syrlybekkyzy, S., Volokitin, A., Nurshakhanova, L., Nurbaeva, F., Kolesnikov, A., Sabyrbayeva, G., Izbassar, A., Kolesnikova, O., Liseitsev, Y., Vavrenyuk, S., 2023b. Increasing strength and performance properties of bimetallic rods during severe plastic deformation. Case Stud. Constr. Mater. 19, e02256. https://doi.org/10.1016/j.cscm.2023.e02256.

Vyas, H.D., Mehta, K.P., Badheka, V., Doshi, B., 2021. Processing and evaluation of dissimilar Al-SS friction welding of pipe configuration: Nondestructive inspection, properties, and microstructure. Measurement 167, 108305. https://doi.org/10.1016/j.measurement.2020.108305.

Wu, H.C., Yeh, W.C., 1991. On the experimental determination of yield surfaces and some results of annealed 304 stainless steel. Int. J. Plast 7, 803–826. https://doi.org/10.1016/0749-6419(91)90019-U.

Yang, C., Shi, B., Peng, Y., Pan, F., 2019. Loading path dependent distortional hardening of Mg alloys: Experimental investigation and constitutive modeling on cruciform specimens. Int. J. Mech. Sci. 160, 282–297. https://doi.org/10.1016/j.ijmecsci.2019.06.046.

Yilmaz, O., Çelik, H., 2003. Electrical and thermal properties of the interface at diffusion-bonded and soldered 304 stainless steel and copper bimetal. J. Mater. Process. Technol. 141, 67–76. https://doi.org/10.1016/S0924-0136(03)00029-3.

Zhou, J., Xu, Y., Lopez, M.A., Farbaniec, L., Patsias, S., Macdougall, D., Reed, J., Petrinic, N., Eakins, D., Siviour, C., Pellegrino, A., 2022. The mechanical response of commercially pure copper under multiaxial loading at low and high strain rates. Int. J. Mech. Sci. 224, 107340. https://doi.org/10.1016/j.ijmecsci.2022.107340.